

2

# NAVAL POSTGRADUATE SCHOOL Monterey, California

AD-A227 258



DTIC  
ELECTE  
OCT 10 1990  
S B D  
Co

## THESIS

VALIDATION OF A COMPUTATIONAL MODEL  
FOR AUTOGENOUS ARC WELDING

by

Eugene B. Sedy

March 1990

Thesis Advisor

Y. Joshi

Approved for public release; distribution is unlimited.

Unclassified

security classification of this page

## REPORT DOCUMENTATION PAGE

1a Report Security Classification <b>Unclassified</b>			1b Restrictive Markings		
2a Security Classification Authority			3 Distribution Availability of Report		
2b Declassification/Downgrading Schedule			Approved for public release; distribution is unlimited.		
4 Performing Organization Report Number(s)			5 Monitoring Organization Report Number(s)		
6a Name of Performing Organization Naval Postgraduate School		6b Office Symbol (if applicable) 34	7a Name of Monitoring Organization Naval Postgraduate School		
6c Address (city, state, and ZIP code) Monterey, CA 93943-5000		7b Address (city, state, and ZIP code) Monterey, CA 93943-5000			
8a Name of Funding Sponsoring Organization		8b Office Symbol (if applicable)	9 Procurement Instrument Identification Number		
8c Address (city, state, and ZIP code)		10 Source of Funding Numbers			
		Program Element No. Project No. Task No. Work Unit Accession No.			
11 Title (include security classification) <b>VALIDATION OF A COMPUTATIONAL MODEL FOR AUTOGENOUS ARC WELDING (Unclassified)</b>					
12 Personal Author(s) Eugene B. Sedy					
13a Type of Report Master's Thesis		13b Time Covered From To		14 Date of Report (year, month, day) March 1990	
15 Page Count 59					
16 Supplementary Notation The views expressed in this thesis are those of the author and do not reflect the official policy or position of the Department of Defense or the U.S. Government.					
17 Cosat Codes			18 Subject Terms (continue on reverse if necessary and identify by block number)		
Field	Group	Subgroup	Welding, Arc, Computer, Modeling, Heat transfer, Fusion zone		
19 Abstract (continue on reverse if necessary and identify by block number) A three dimensional transient computational model of heat transfer during gas tungsten arc welding is generalized, and then validated by comparison to Rosenthal's solution for moving point sources of heat. The current version of the code allows much greater flexibility in the specification of the thermal input from the arc. The resulting surface temperature profiles and fusion zone shapes are compared to those measured experimentally for several input power levels for autogenous gas tungsten arc welding. Arc efficiency is experimentally determined using change of phase of a liquid fluorocarbon. The model is shown to be useful for modeling autogenous welding of thick plates. Weld seam misalignment and surface flaw detection are shown to be possible ahead of the arc with accurate surface temperature detection methods. The potential of the model for creating a database of fusion and heat affected zone sizes, temperature profiles, and cooling rates for various materials, processes, and power levels is indicated.					
20 Distribution Availability of Abstract <input checked="" type="checkbox"/> unclassified unlimited <input type="checkbox"/> same as report <input type="checkbox"/> DTIC users			21 Abstract Security Classification Unclassified		
22a Name of Responsible Individual Y. Joshi			22b Telephone (include Area code) (408) 646-3400		22c Office Symbol 69Jj

Approved for public release; distribution is unlimited.

Validation of a Computational Model for Autogenous Arc Welding

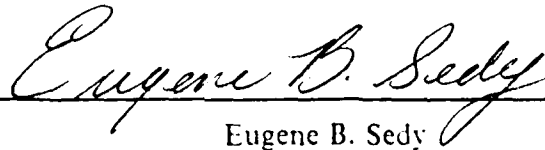
by

Eugene B. Sedy  
Lieutenant, United States Navy  
B.S.A.E., United States Naval Academy, 1981

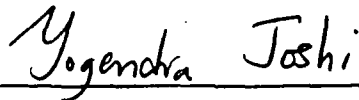
Submitted in partial fulfillment of the  
requirements for the degrees of

MASTER OF SCIENCE IN MECHANICAL ENGINEERING  
and  
MECHANICAL ENGINEER  
from the  
NAVAL POSTGRADUATE SCHOOL  
March 1990

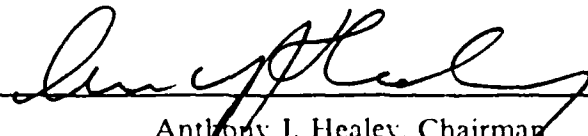
Author:

  
Eugene B. Sedy

Approved by:



Y. Joshi, Thesis Advisor



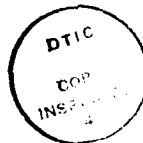
Anthony J. Healey, Chairman,  
Department of Mechanical Engineering



DEAN OF FACULTY  
AND GRADUATE STUDIES

## ABSTRACT

A three dimensional transient computational model of heat transfer during gas tungsten arc welding is generalized, and then validated by comparison to Rosenthal's solution for moving point sources of heat. The current version of the code allows much greater flexibility in the specification of the thermal input from the arc. The resulting surface temperature profiles and fusion zone shapes are compared to those measured experimentally for several input power levels for autogenous gas tungsten arc welding. Arc efficiency is experimentally determined using change of phase of a liquid fluorocarbon. The model is shown to be useful for modeling autogenous welding of thick plates. Weld seam misalignment and surface flaw detection are shown to be possible ahead of the arc with accurate surface temperature detection methods. The potential of the model for creating a database of fusion and heat affected zone sizes, temperature profiles, and cooling rates for various materials, processes, and power levels is indicated.



<b>Accession For</b>	
NTIS GRA&I	<input checked="" type="checkbox"/>
DTIC TAB	<input type="checkbox"/>
Unannounced	<input type="checkbox"/>
Justification	
By _____	
Distribution/	
Availability Codes	
Dist	Avail and/or Special
A-1	

## TABLE OF CONTENTS

I. INTRODUCTION .....	1
II. MODIFICATIONS TO THE MODEL CODES .....	6
A. MATERIAL AND GRID PARAMETERS .....	6
B. GAUSSIAN DISTRIBUTED HEMISPHERICAL HEAT INPUT .....	6
C. LACK OF FUSION PROGRAMS .....	8
D. SURFACE HEAT INPUT .....	11
E. DOUBLE ELLIPTICAL HEAT INPUT .....	11
F. ROSENTHAL VERIFICATION CODE .....	14
G. COOLING RATE CODE .....	16
III. EXPERIMENTAL APPARATUS .....	19
A. WELDING MACHINE .....	19
B. PLATE INSTRUMENTATION .....	19
C. DATA ACQUISITION SYSTEM .....	19
D. ARC EFFICIENCY DETERMINATION .....	21
E. FUSION ZONE COMPARISON .....	22
IV. EXPERIMENTAL RESULTS .....	24
A. DETERMINATION OF POWER INPUT TO SAMPLE .....	24
B. TEMPERATURE-TIME PLOT COMPARISONS .....	24
C. FUSION ZONE COMPARISON .....	26
D. SURFACE FLAW COMPARISON .....	32
E. EXPERIMENTAL UNCERTAINTIES .....	32
1. Efficiency determination .....	32
2. Fusion zone comparison .....	34
V. RECOMMENDATIONS .....	36
A. COOLING RATE CONTROL .....	36
B. HEAT INPUT DISTRIBUTION .....	36
C. FLAW DETECTABILITY .....	36

D. TEMPERATURE SENSING SYSTEM .....	36
APPENDIX A. FLOW CHART .....	37
APPENDIX B. MODIFIED PROGRAMS .....	39
A. BASIC MODIFICATIONS .....	39
1. START2 Program Modified Sections .....	39
2. Variable List .....	41
3. Original WELD Program Sections .....	42
LIST OF REFERENCES .....	45
BIBLIOGRAPHY .....	47
INITIAL DISTRIBUTION LIST .....	49

## LIST OF TABLES

Table 1. FUSION ZONE COMPARISON .....	26
---------------------------------------	----

## LIST OF FIGURES

Figure 1.	Surface temperature profiles varying the constant in the Gaussian factor	9
Figure 2.	Arc-to-flaw distances	10
Figure 3.	Per cent difference temperatures of surface flaws	12
Figure 4.	Temperature profiles for low and high conductivity flaws	13
Figure 5.	Rosenthal verification results	15
Figure 6.	Cooling rates comparison	17
Figure 7.	Thermocouple locations	20
Figure 8.	Welding and data acquisition systems	21
Figure 9.	Efficiency determination system	23
Figure 10.	Welding process efficiency	25
Figure 11.	Fusion zone comparison at 0.5 seconds	27
Figure 12.	Fusion zone comparison at 1.5 seconds	28
Figure 13.	Fusion zone comparison at 2.0 seconds	29
Figure 14.	Fusion zone comparison at 3.0 seconds	30
Figure 15.	Fusion zone comparison over time	31
Figure 16.	Surface flaw temperature-time plots	33
Figure 17.	Noise in the thermocouple output	35
Figure 18.	Program Flow Chart	38



## I. INTRODUCTION

The pursuit of an automatic adaptive control system for the gas tungsten arc welding (GTAW) process has been ongoing for nearly two decades. Numerous researchers have assisted in developing the state of the art during this time. However, the pursuit continues, as many of the so-called automatic welders are not truly automatic; an experienced, highly-skilled operator is the key to the success of these "automatic" welders.

To design a completely automatic system, the first step is to model the process as accurately as possible. To obtain an accurate model, all aspects of the process must be fully understood. Once the process is understood, mathematical formulas can be developed expressing the relationships between the variables in the process. Perhaps the first and the most well known of the many models is that of Rosenthal [Ref. 1]. His model of the process is the analytic solution of the heat diffusion equation in the presence of point, line, and plane moving sources of heat. More recent work has shown that while Rosenthal's solutions are reasonable approximations of reality far away from the heat sources, in the vicinity of the fusion zone these are in considerable error. Effects of melting and the resulting variations in the thermophysical and transport properties must be accounted for in addition to a heat source of finite size in order to estimate the time temperature histories.

The advent of modern control theory, nearly a decade ago, created the opportunity to advance the modeling of GTAW and gas metal arc (GMA) welding processes. Moody was perhaps the first to publish models of the GMA and GTA welding processes in the state-space. He presented descriptions of the process variables and the resulting nine first order non-linear differential equations relating the variables. His work appears to be the starting point for a fully automatic system. One only has to determine the exact nature of the relationships to create the system. The effort to determine these relationships sums up the next decade or so of research in the area of automatic control of welding. Not all of the variables in Moody's model are measurable, which is not a problem as long as the unmeasurable variables can be estimated through the use of empirical relationships, or some other means. Once all variables are measured or estimated, a closed loop control system may be designed using the relationships between the variables and their derivatives. [Ref. 2]

A refinement of Rosenthal's solution, using all but one of his assumptions was presented by Eagar and Tsai in 1983. The assumption not used was the point source of heat. Eagar and Tsai used a distributed source of heat with a Gaussian distribution. The comparison of their results with experimental data revealed a closer agreement than Rosenthal's analysis. They concluded that the strength of the theory presented was that it gave accurate functional relationships between process parameters and materials parameters. [Ref. 3]

At nearly the same time, Goldak *et al.* were developing a finite element model for welding. In their paper they take the concept of a distributed source a few steps further by applying it over a volume of the work piece to account for the arc digging and stirring. They note the limitations of applying a disk source at the surface of the material to a deeply penetrating process such as electron beam welding. Thus the hemispherical power density distribution model is proposed. Then, noting that few if any actual molten pools are hemispherical, they proposed an ellipsoidal power density distribution. This idea was further generalized to a double ellipsoidal power density distribution. This came about because the asymmetry of the temperature gradients ahead and behind the arc were not closely matched by the ellipsoidal model. The double ellipsoidal model allows for using quadrants of two different ellipsoids, front and rear, to more closely model actual results. The power of this model for modeling seam welding of two dissimilar metals by splitting the quadrants into octants down the arc centerline was noted. [Ref. 4]

Kou and Sun studied the fluid flow during stationary welding, to later apply their results to moving sources of heat. The driving forces for fluid flow in the weld pool for aluminum and steels were listed in order of their relative effect on the flow pattern. Their work could provide substantial evidence for use in determining the dimensions of a double-ellipsoidal power distribution region for a given set of process parameters once their results are applied to moving arcs. [Ref. 5]

Tsai and Eagar related current, arc length, electrode tip angle, and shielding gas composition to heat input magnitude and heat source distribution. The arc length was shown to be the most effective in shaping the heat distribution and the current was shown to dominate the magnitude of the heat flux on the surface. They also determined that the heat flux was closely approximated by a Gaussian distribution and gave the approximate range of the distribution half-width as arc length was increased. [Ref. 6]

Kou and Wang achieved excellent agreement between predicted and measured weld pool shapes using a three-dimensional computer simulation of convection in the weld

pool. The only drawback to their work was that symmetry was invoked, which removes the ability to model asymmetrical problems associated with welding such as weld seam-electrode misalignment. [Ref. 7]

The effects of changes in machine variables were investigated at length by Giedt. The wide range of efficiencies of the GTA process was explained as due to the fact that conduction heat transfer models do not take into account the convective heat transfer in the weld pool. Giedt also listed some computing time requirements of interest. Using TACO3D, a three-dimensional finite element conduction heat transfer code, with constant average thermal properties, one hour of CRAY computer time was used. This was increased to nearly ten hours using variable properties and a smaller element size to smooth contours. One of Giedt's conclusions is that the effect of weld pool convection cannot be accurately represented in a pure conduction model. He notes that use of a fictitiously higher thermal conductivity (2 to 5 times that of the solid) has been used to account for the effect of convection, but the applicability of doing so is dependent on the direction of flow in the weld pool, which may not be known. [Ref. 8]

Oreper and Szekely examined the development of the weld pool for a tungsten inert gas (TIG) spot weld. They noted that during the initial period of the arc, convection played very little part, and became more significant as time went on. This behavior was not common to all materials. For titanium, neglecting convection in the weld pool initially would cause large errors. Three guidelines were presented:

- convection is not likely to be important for good conductors and shallow weld pools.
- convection is likely to be important for poor conductors and deep weld pools
- surface tension effects are likely to be important in affecting the circulation pattern and subsequent weld pool shape.

The conclusions stated were that the conditions for which convection plays an important part can be defined and that the relative importance of surface tension, buoyancy and electromagnetic forces in determining the weld pool shape and circulation patterns can be determined. [Ref. 9]

Lu and Kou used a technique called non-parametric minimization to determine the power and current distributions in a gas tungsten arc. This technique was applied to the split anode method. They noted that the power- and current-density distributions in gas tungsten arcs are generally steeper than the Gaussian distribution, making it a poor approximation in the case of a larger arc gap. The Gaussian distribution was fairly close for the smaller arc gaps. [Ref. 10]

Zacharia *et al.* developed a computational model code called WELDER. The code has nine special features which allow it to realistically simulate many interesting problems including inclined welding and welding in microgravity environments. The code takes into account the following physical phenomena:

- melt surface is deformable--the weld crown, surface ripples and surface gravity wave phenomena can be simulated.
- the local transient effect of phase transformation is incorporated into the energy equation.
- marked-element technique--accurately simulates transient development of the solid-liquid interface.
- incorporates effect of surface tension due to local curvature conditions of the deformable surface of the molten metal.
- considers the magnetohydrodynamic force terms in the momentum equation.
- ability for motion of the arc and arbitrary positions (inclined welding).
- different gravitational forces.
- arbitrary geometry and finite thickness.
- does not require use of the Boussinesq approximation.

The capabilities of the code appear to be extensive. CPU times of about 30 minutes were reported, but not correlated to the amount of real time simulated. Since the sample size (24mm by 24mm by 6mm) and material (Al 6061) properties may have had a significant effect on the CPU time required, obtaining timely results for a wide range of processes and materials is uncertain. [Ref. 11]

Zacharia *et al.* reported on the influence of surface active agents and the temperature distribution on the weld pool surface. It was concluded that penetration and the weld pool aspect ratio were dependent on a combination of the two factors. The sulfur contents (90 ppm and 240 ppm) had a significant effect on the weld penetration for the GTA process for 304 stainless steel, however, there was no noticeable difference for the laser beam process which was also investigated. [Ref. 12]

A three-dimensional numerical model of the Gas Tungsten Arc (GTA) welding process was created by Ule [Ref. 13], as a tool for the development of an expert welding system. The David Taylor Research Laboratory is developing such a system for welding submarine hulls. Before using Ule's model in any application, extensive testing and validation was required.

Testing the numerical model's Fortran codes was accomplished in several steps. These included:

- Comparing the expressions in the Fortran codes to the governing equations.
- Running the programs.
- Comparing the output to previously published output.

The validation of the model also consisted of several steps. These were:

- Determination of the arc efficiency of the GTA process.
- Comparison of the surface temperature profiles with the profiles from the Rosenthal solution with the same heat input.
- Comparison of the surface temperature profiles with the instrumented plate experimental results for the same heat input.
- Comparison of weld pool shapes during start-up from experimental results with shapes predicted by the codes.

The model was shown to be useful in predicting the temperature distribution during GTA welding. There is continuing research to verify cooling rates during welding start-up and shutdown and to develop a low-cost surface temperature sensing system. Completion of these research efforts will facilitate the design and subsequent use of an expert welding system for GTA welding which with some effort could be adapted to the Gas Metal Arc (GMA) welding process.

## II. MODIFICATIONS TO THE MODEL CODES

### A. MATERIAL AND GRID PARAMETERS

The first modification to Ule's basic welding program [Ref. 13: pp. 84-92], was to replace parameters which had been hand calculated and entered as constants, with variable expressions, thus allowing changes in material and welding parameters to be more easily effected. Examples of the parameters that were changed in the way they were represented in the code are:  $Fo(1)$ ,  $Fo(2)$ ,  $Fo(3)$ ,  $Bi(1)$ ,  $Bi(2)$ ,  $Bi(3)$ ,  $Bi(4)$ . To make changes to these variables required the introduction of eighteen additional variables in the program. Since these variables were involved in calculations only once, the additional cost in computation time was negligible. The changes in the  $Fo(1)$  expression demonstrate how the code was modified for the variables listed above. The  $Fo(1)$  expression in Ule's program WELD was:

$$Fo(1) = 0.1636\Delta t$$

The revised expression used in the START series of programs and all subsequent revised codes used the following expression:

$$Fo(1) = \frac{\alpha \Delta t}{\Delta x_c \Delta y_c (.001)^2}$$

where:

- $\alpha$  is the diffusivity
- $\Delta t$  is the time step
- $\Delta x_c$  is the control volume length in the x-direction in the coarse zone
- $\Delta y_c$  is the control volume length in the y-direction in the coarse zone
- $(.001)$  converts from millimeters to meters

Similar changes were made to the other Fourier and Biot numbers.

### B. GAUSSIAN DISTRIBUTED HEMIISPHERICAL HEAT INPUT

The most significant change to the codes was the manner in which the heat was input to the metal. Ule had used a Gaussian distribution over a rectangular parallelepiped, though the volume was stated to be hemispherical [Ref. 13: pp. 14,86]. The START2 code was a version of WELD modified to simulate a hemispherical heat input of 4.5

millimeter radius, with a Gaussian distribution. The Gaussian distribution was modeled using the approach outlined by Goldak *et al.* [Ref. 4: pp. 301-302] for a finite element model. The discretized equation for heat input per unit volume became:

$$H_{i,j,k}^{n+1} = H_{i,j,k}^n + \frac{Q G_{i,j,k}}{\sum G_{i,j,k} V_{i,j,k}}$$

where:

- n** is the current time level
- i,j,k** are the nodal indices
- $G_{i,j,k}$**  is the Gaussian factor,  $e^{-3((\frac{x}{a})^2 + (\frac{y}{b})^2 + (\frac{z}{c})^2)}$
- $V_{i,j,k}$**  is the nodal volume
- Q** is the power input in watts
- $H_{i,j,k}$**  is the enthalpy per unit volume at a particular time

It was noted that the constant in the exponent of the Gaussian factor was 1.7 in Ule's codes [Ref. 13: p. 86] which corresponds to a relative intensity of the arc power of about 18.3 per cent at the edge of the arc, vice five per cent as suggested by Goldak *et al.* [Ref. 4: p. 301]. Using three as the constant gives a five per cent value at the arc boundary. An investigation as to the effect of the exponent on the surface temperature profiles was made. The exponent was varied between 1.0 and 3.0 in increments of 0.5 and the resultant surface temperature profiles plotted and visually compared. It was noted that the size and shape of the weld pool (near the 1750 K isotherm) was virtually unchanged. The differences between the plots were the temperature gradients and peak temperatures within the weld pools. As expected, both were higher for the more concentrated heat input (using three as the constant). A collection of the plots is provided in Figure 1. The variable GAUSS refers to the constant in the exponent.

Fourteen more variables were added to code this equation. The values of *a*, *b*, and *c* are the *x*, *y*, and *z* radii of the arc power distribution in millimeters, respectively for a continuous model. Discretizing the model enlarges the radii in the *x*- and *y*-directions and decreases the radius in the *z*-direction by one-half the nodal spacing, or 0.5 millimeters in this case. The limits of summation for the above equation were found by dividing *a*, *b*, and *c* by the node spacing and adding and subtracting this value plus one to the arc center. The one was needed to ensure that no nodes were left out since the arc position in the *y*-direction was discretized by the Fortran function INT.

Adding the one also allows for values of the arc radius other than those ending in .5 and for changes in the  $x$ -position of the arc as occur in the misalignment programs. As an example, the limits of summation for a 4.5 millimeter radius hemispherical heat input were:

$x$	from $XARC-5$ to $XARC+5$
$y$	from $YARC-5$ to $YARC+5$
$z$	from 1 to 5

### C. LACK OF FUSION PROGRAMS

The lack of fusion program, WELDLF, was first altered to input the heat of the arc in a hemispherical fashion identical to the START series. The temperature deviations from quasi-steady conditions oscillated excessively near the flaw zone. Diagnostic testing revealed that the variable LOF, used to control the position of the lack of fusion zone, was incorrectly determined. The equation used by Ule [Ref. 13: p. 33] was

$$LOF = 65 - INT(VEL \times TIME)$$

which moves the flaw in one millimeter increments as the distance changes. The error arises from the fact that the arc is also moving toward the flaw. To correct this, the flaw was moved only when the fine zone was shifted, thus ensuring the flaw maintained a fixed position in the metal. The equation used in WELDL1 and subsequent revisions used a variable already defined.

$$LOF = 67 - STEP$$

The variable STEP is incremented by three each time the fine zone is shifted. The difference between the two methods of placing the flaw in the material is illustrated by the plots in Figure 2. The  $YARC-JMIN$  curves represent the distance from the arc to the node at the front of the flaw; the  $YARC-JMAX$  curves the distance from the arc to the rear of the flaw. The front of the flaw is the edge nearest the arc when the flaw is introduced into the material. The distance between the curves on each plot corresponds to the distance between the first and last nodes of the flaw. The actual flaw distance is one node spacing longer, or 4mm in this case. The effect of the change in the LOF variable on surface differential temperature profiles is demonstrated by the plots in



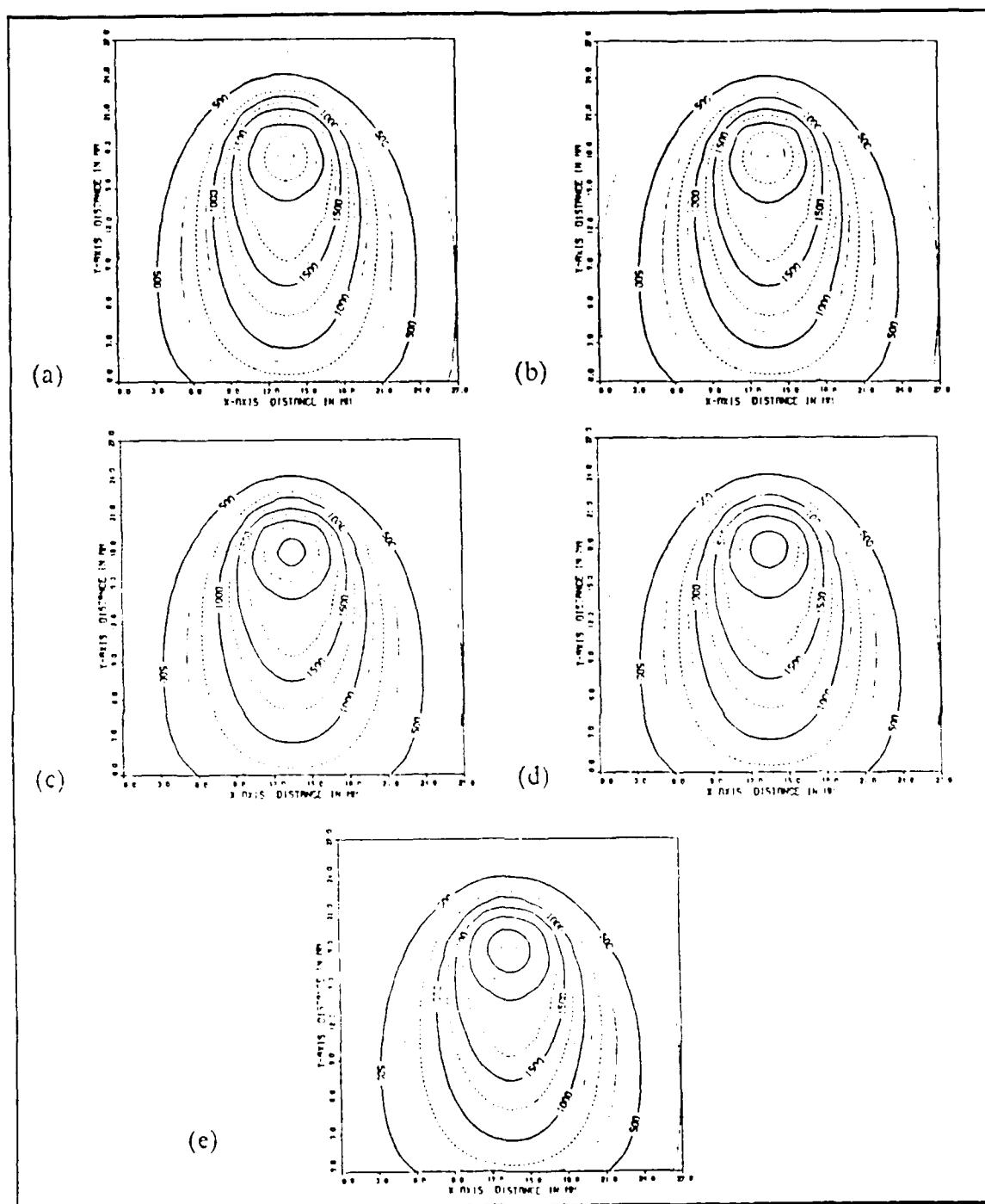


Figure 1. Surface temperature profiles varying the constant in the Gaussian factor: a) GAUSS = 1.0, b) GAUSS = 1.5, c) GAUSS = 2.0, d) GAUSS = 2.5, e) GAUSS = 3.0

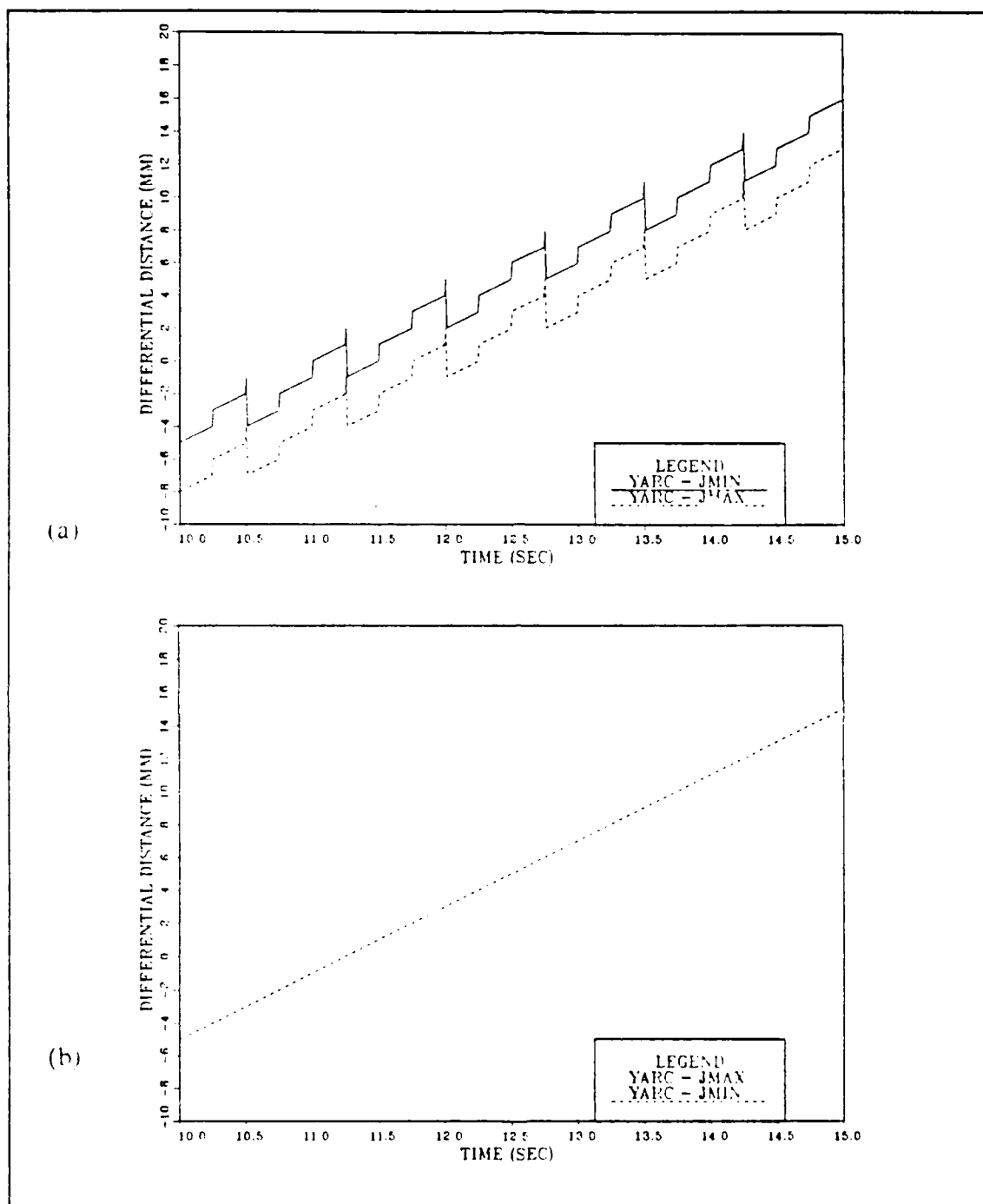


Figure 2. Arc-to-flaw distances: (a) incorrect LOF variable (b) correct LOF variable

Figure 3. This change removed much of the jaggedness of the plotted differential surface temperatures near the flaw.

An additional change to the WELDL series was the thermal conductivity of the flaw. No material could be found with an extremely low conductivity for which thermal conductivity and heat capacity versus temperature relationships over the range of temperatures encountered during the welding process were available. The conductivity was therefore set arbitrarily to a constant  $5.0 \text{ W/m} \cdot \text{K}$  and the heat capacity to the same relationship as the parent material. This was done in order to examine the effect of a low thermal conductivity inclusion on the temperature variation within the material.

A high conductivity flaw material was also utilized, in a different version of the WELDL code series. The material chosen was tungsten. Piecewise linear relationships were fit to data from a table in Incropera and DeWitt [Ref. 13] for the thermal conductivity and specific heat of tungsten. While the thermal properties of the flaws encountered in applications may vary, the intent in this study was to determine the response of the temperature patterns to a flaw of thermal conductivity higher than the parent material. Plotted results comparing the low and high conductivity flaws are included in Figure 4.

#### **D. SURFACE HEAT INPUT**

The program STARSU was utilized to obtain the results of a surface heat input. In this case, the heat was input only to the surface nodes in a Gaussian distribution over circle of radius  $4.5\text{mm}$ . The depth radius was set to zero and the code altered to prevent division by zero.

The results of the surface heat input were unrealistic. The maximum temperatures experienced in the weld pool were near  $4000 \text{ K}$ . One interesting point was that the size and shape of the weld pool boundary was relatively unchanged from that obtained for the hemispherical heat input.

#### **E. DOUBLE ELLIPTICAL HEAT INPUT**

A version of the START program, STARDE, was used to observe the effect of a double elliptical heat distribution. The program was altered to include the discretized form of the equation presented by Goldak *et al.* [Ref. 4: p. 302]. The double ellipsoid used had a  $9.0\text{mm}$  minor axis ( $x$ -directions), semi-major axes of  $4.5\text{mm}$  to the front ( $+y$ -direction) and  $8.5\text{mm}$  to the rear ( $-y$ -direction) and a  $1.5\text{mm}$  depth ( $z$ -direction). The heat was input using a Gaussian distribution with 70 per cent of the net input in the rear portion of the ellipsoid and 30 per cent in the front portion. The size and shape of

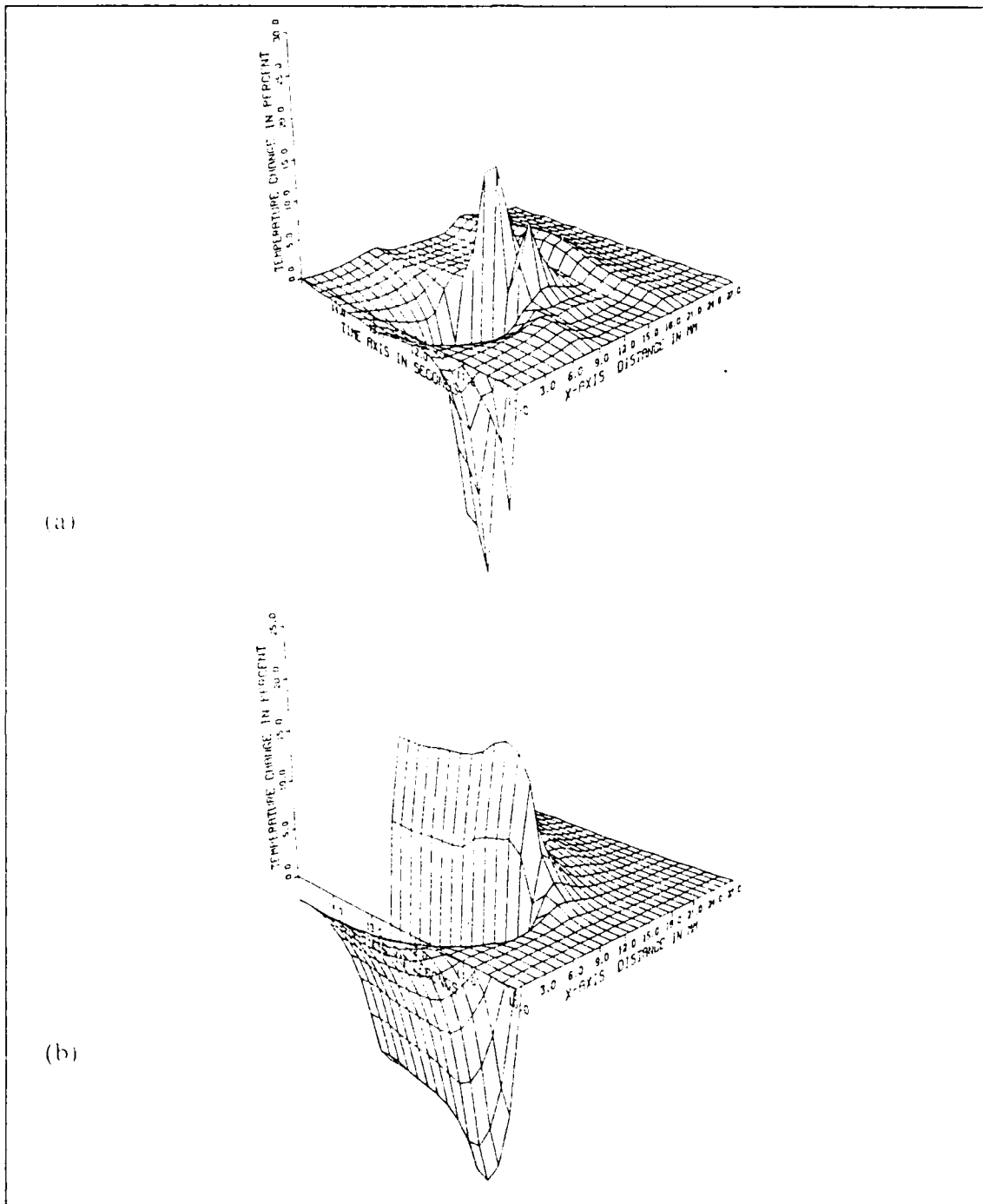


Figure 3. Per cent difference temperatures of surface flaws: (a) incorrect LOI variable, (b) correct LOI variable

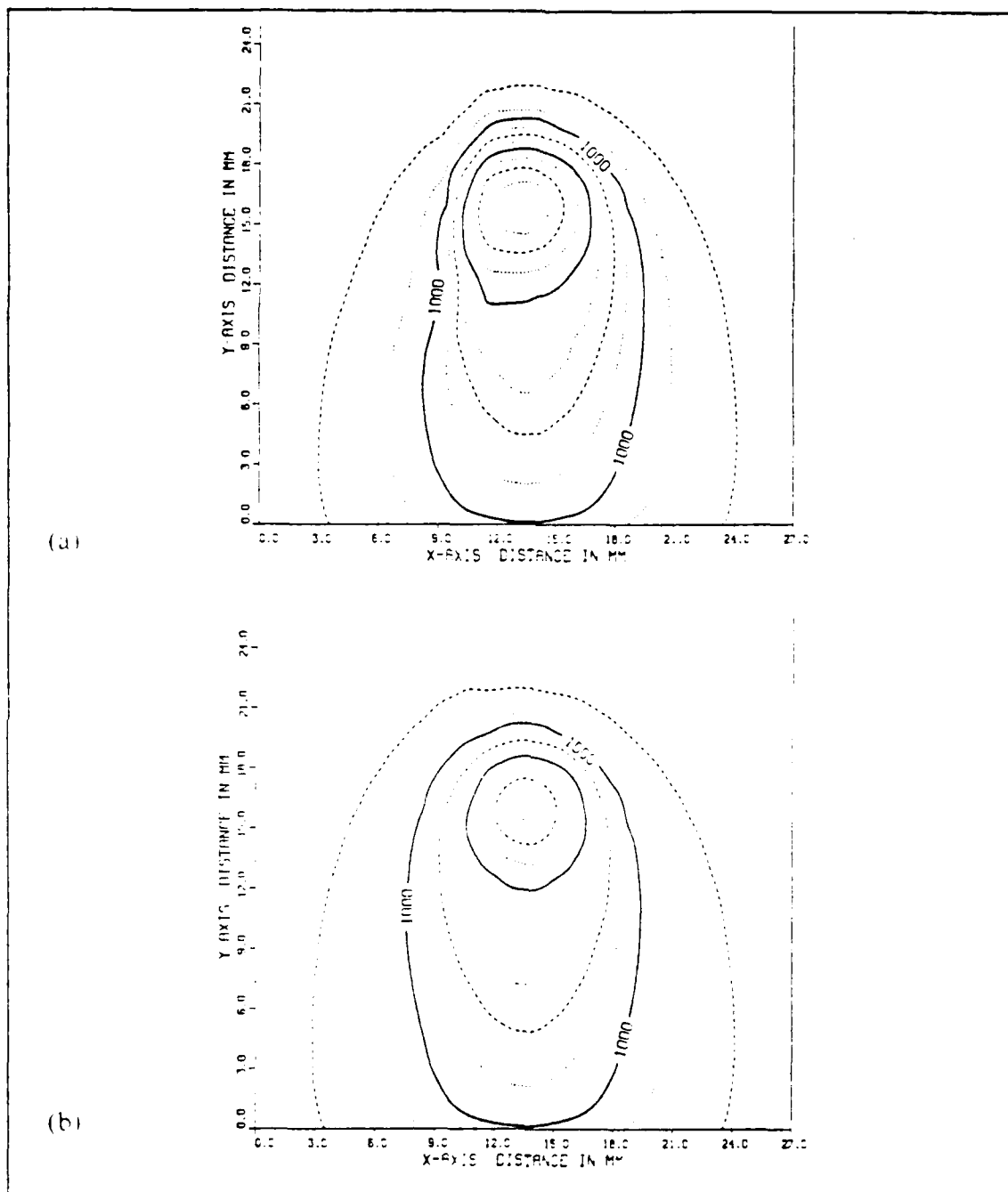


Figure 4. Temperature profiles for low and high conductivity flaws: (a) low conductivity flaw, (b) high conductivity flaw

the distribution as well as the front and rear fractions were arbitrary, but not without knowledge of the values chosen in other programs for the laser welding process.

The plotted results were compared to the rectangular parallelepiped, hemispherical, and surface heat inputs. It was noted that the size and shape of the fusion zone on the surface was not changed much between the surface and hemispherical heat inputs. The double elliptical heat input resulted in more oblong weld pools than the other methods. The ratio of the semi-major axis ahead of the arc to that behind the arc may have been too high as the temperature gradients were not as steep in front of the arc as would be expected. The cross sections of the fusion zones were more noticeably different. The hemispherical heat input resulted in profiles which appeared deeper than the half-width of the fusion zone at the surface. The double elliptical heat input resulted in fusion zones with depths less than the half-width at the surface, which was found to be close to the shapes observed in later experiments.

#### **F. ROSENTHAL VERIFICATION CODE**

The program STARTR was created from the START series to simulate the Rosenthal solution [Ref. 1: pp. 849-869]. This was accomplished in the following manner:

- reducing the heat input to prevent melting
- using constant thermal properties (conductivity and specific heat)
- eliminating convection and radiation from the surfaces
- adding the heat to a single node on the surface

The Rosenthal solution was coded in the program ROSEN and the output compared to the STARTR output using plots from a revised plotting program. These plots appear in Figure 5.

Rosenthal surface temperature profiles which would have included the infinite point (the center of the arc) were drawn using a point-to-point curve drawing routine with the infinite point replaced by a large finite value, while all other plots used a natural spline curve drawing routine.

The model adequately predicted the temperatures at the four locations chosen. The errors were maximum at the center of the arc where the Rosenthal solution is known to be lacking in its representation of actual conditions. Other than the center of the arc, the maximum difference between the model results and the analytic solution was about one degree which translates to less than one per cent.

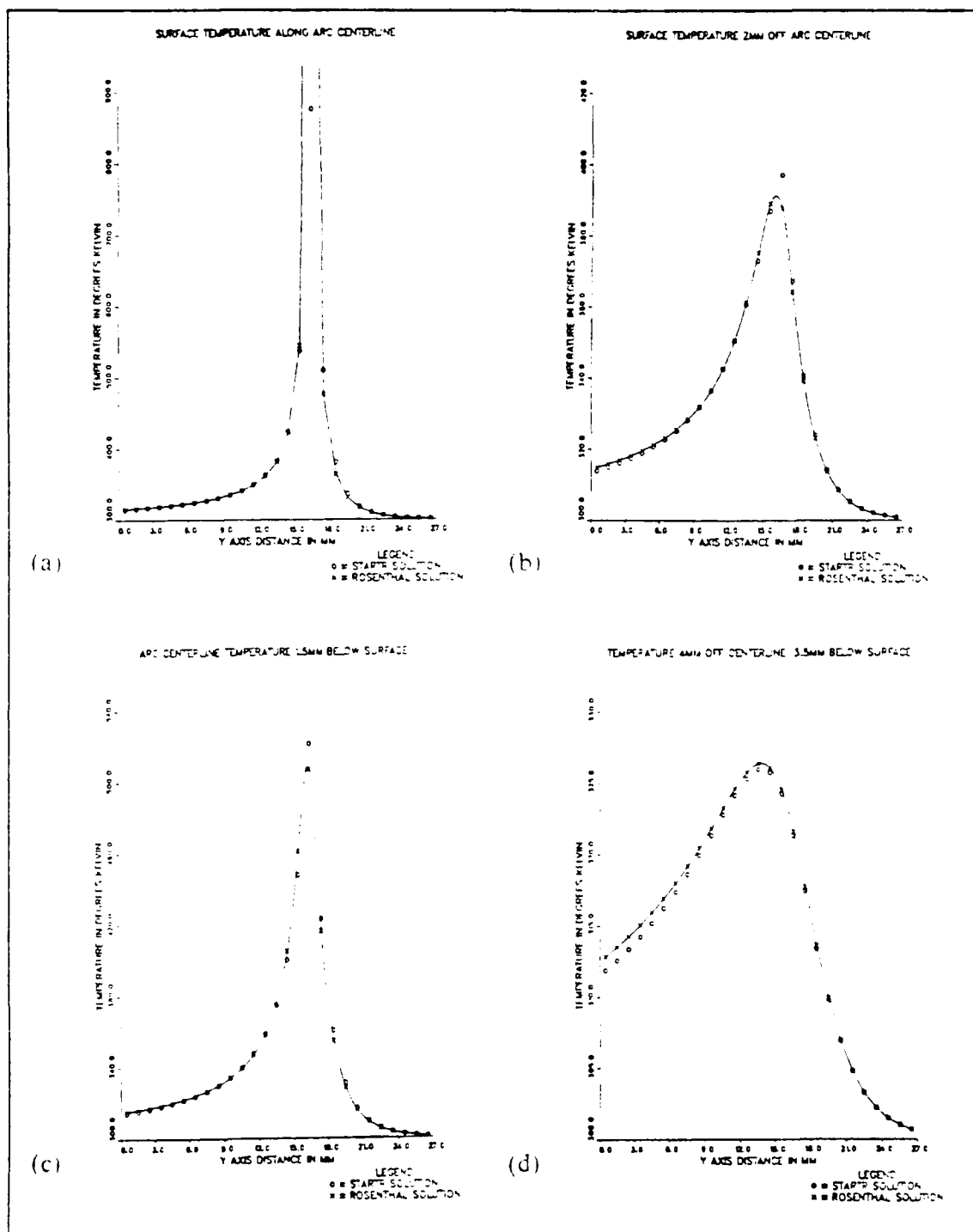


Figure 5. Rosenthal verification results

## G. COOLING RATE CODE

The program created by Ule [Ref. 12: pp. 127-134] to determine the cooling rates during the welding process was modified by changing the heat input to a Gaussian distributed hemisphere as was done for the previous codes. Giedt [Ref. 8: pp. 35, 39-40] had pointed out that modeling the process with a pure conduction model was inaccurate, but that some reasonable results had been obtained in a conduction model by adjusting the thermal conductivity of the liquid metal. It was also pointed out that the weld pool circulation pattern must be known to properly account for convection when using a conduction model. Taking these points into account, a new version of the code, WELDC1, was written. The heat was input on the surface in a 4.5 mm radius until a weld pool the approximate width of the quasi-steady state pool formed and then input in a 4.5mm hemisphere. This heat input scheme caused cooling rates about 5 to 7 times higher than for the constant hemispherical input. This occurred because the heat input when concentrated on the surface caused temperatures in excess of 4000 K. When the heat input was shifted to the hemispherical distribution, the sudden diffusion of the heat input resulted in higher cooling rates. To alleviate this problem, the code was altered to input the heat on the surface until the weld pool width exceeded 1mm, then input the heat in an ellipsoid of 4.5mm radius and 1.5mm depth. As the weld pool width at the surface increased, the depth of the heat input was also increased until the depth was 3.5 mm. For a heat input of 1950 watts, the increases in depth of the heat input distribution occurred at 0.08, 0.30, and 2.22 seconds after initiation of the arc. A comparative plot of the two cases above is provided in Figure 6. The parameters used were 1950 watts and 4mm per sec for both plots. The first plot is for a 15 second run with no cooldown; the second for seven seconds of welding followed by eight seconds with no heat input. In the first case, cooling rates of nearly 1400°C per second were predicted near the point of arc initiation. In the second case, the predicted cooling rates were less than 400°C per second at the same point.

Comparing the results of the two cases above with those of Ule [Ref. 12: pp. 44-45], (where a surface input of heat and a directional thermal conductivity in the weld pool were utilized), it became apparent that the cooling rates determined by the model during the initiation of welding were heavily dependent on the heat distribution chosen. To adequately model this part of the weld cycle without taking convection in the weld pool as well as other important phenomena into consideration would require an excessive computational effort using a pure conduction model. The derivation of an empirical relationship that could be used with minimal error would require in-depth study of the



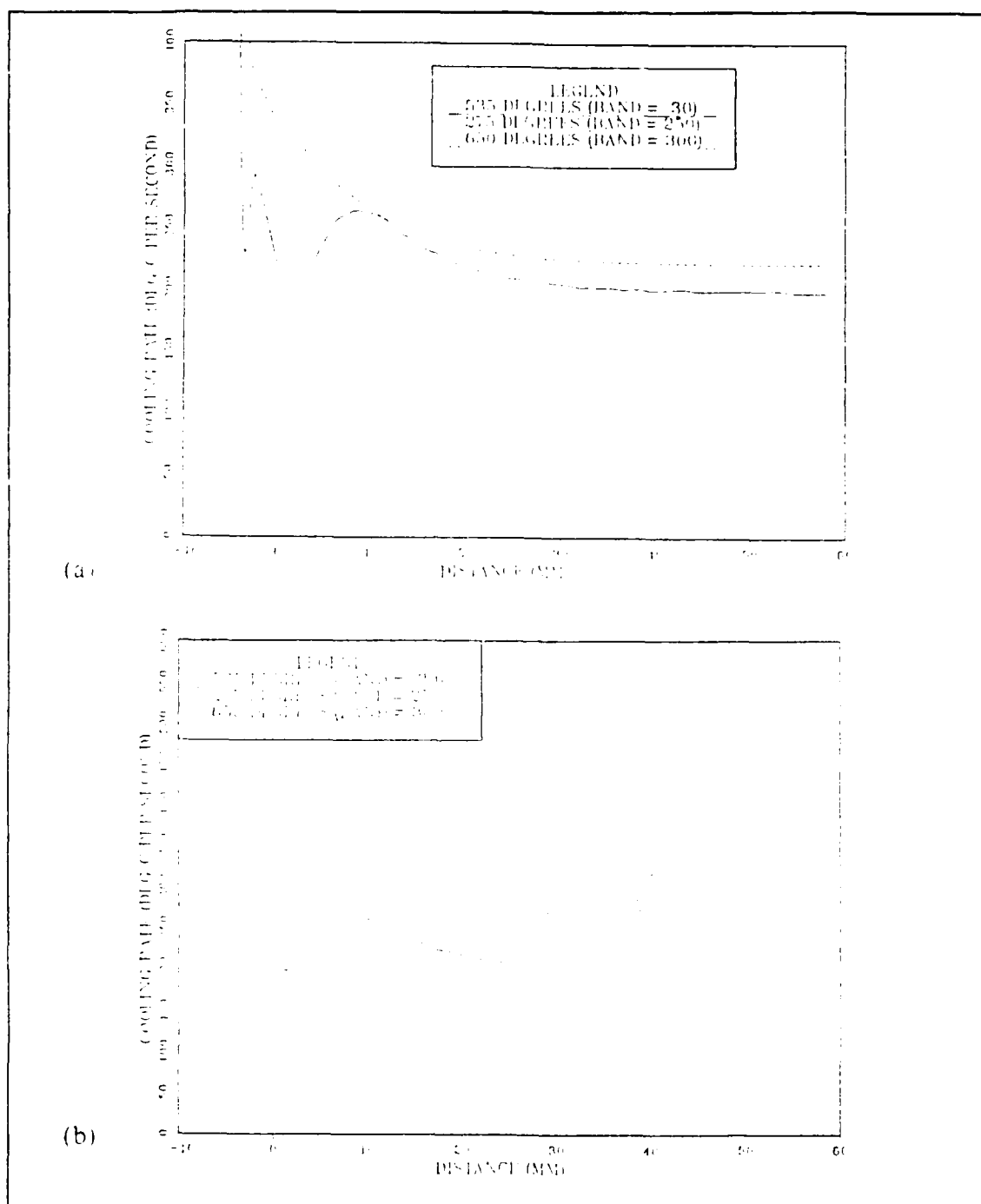


Figure 6. Cooling rates comparison: (a) Step change from surface to hemispherical input (b) Gradual change from surface to hemispherical input

shapes of weld pools from start-up to quasi-steady state for the range of materials and process parameters expected to be encountered. Nearly the same argument can be applied to the cooling rates at arc shutdown.

The use of the codes to correctly determine the actual cooling rates during start-up and shutdown without some accounting for convection and other effects does not appear to be viable. The quasi-steady state cooling rates determined by the model do not suffer from the same limitations.

### **III. EXPERIMENTAL APPARATUS**

#### **A. WELDING MACHINE**

The welding machine utilized for all welds performed during experimentation was a Miller DC Welding Power Source, Model SR600 SCM1A with Electroslope 3. A traverse was included in the setup which allowed for three-dimensional positioning of the electrode. The forward and reverse directions were controlled by a motor. The transverse movement was manual and was only utilized during initial positioning of the torch. The vertical movement was also motor controlled, but not energized during welding. The welding machine was capable of providing direct current up to 675 amperes as well as a high frequency alternating current used to start the arc. The shielding gas used was pure Argon at flow rates of 15 to 20 cubic feet per hour.

#### **B. PLATE INSTRUMENTATION**

The seven- by twelve-inch, one inch thick HY-80 plates were instrumented with up to six platinum-platinum rhodium (type S) thermocouples, three mils in diameter. The thermocouple diameter was chosen as small as practicable to reduce response time. The placement of the thermocouples was as close to the arc centerline as the arc temperature would allow. The distance to the arc of the nearest thermocouple was 12 mm for the baseline runs and 10 mm for the surface flaw runs. The thermocouples were spaced at 3 mm intervals. A diagram of the placement of the thermocouples is shown in Figure 7. The locations were marked by indenting the plates slightly with a punch. A high temperature, high thermal conductivity epoxy, CERAMABOND 569, was used to glue the thermocouples in place. The leads were thread through small ceramic capillaries which provided support for the fragile wires. A wooden support was manufactured for the capillary tubes and the connectors. This arrangement proved very durable and numerous runs were performed on the same plate.

#### **C. DATA ACQUISITION SYSTEM**

The thermocouples were connected to a high speed voltmeter with automatic compensation in an HP3852A Data Acquisition Control Unit. The HP3852A was controlled by an HP9000 series 300 computer with a 9153C 20Mb hard disk and disk drive using Basic version 4.0. The program used to sample the data was existing and had been used extensively for welding laboratory experiments in support of a graduate course.

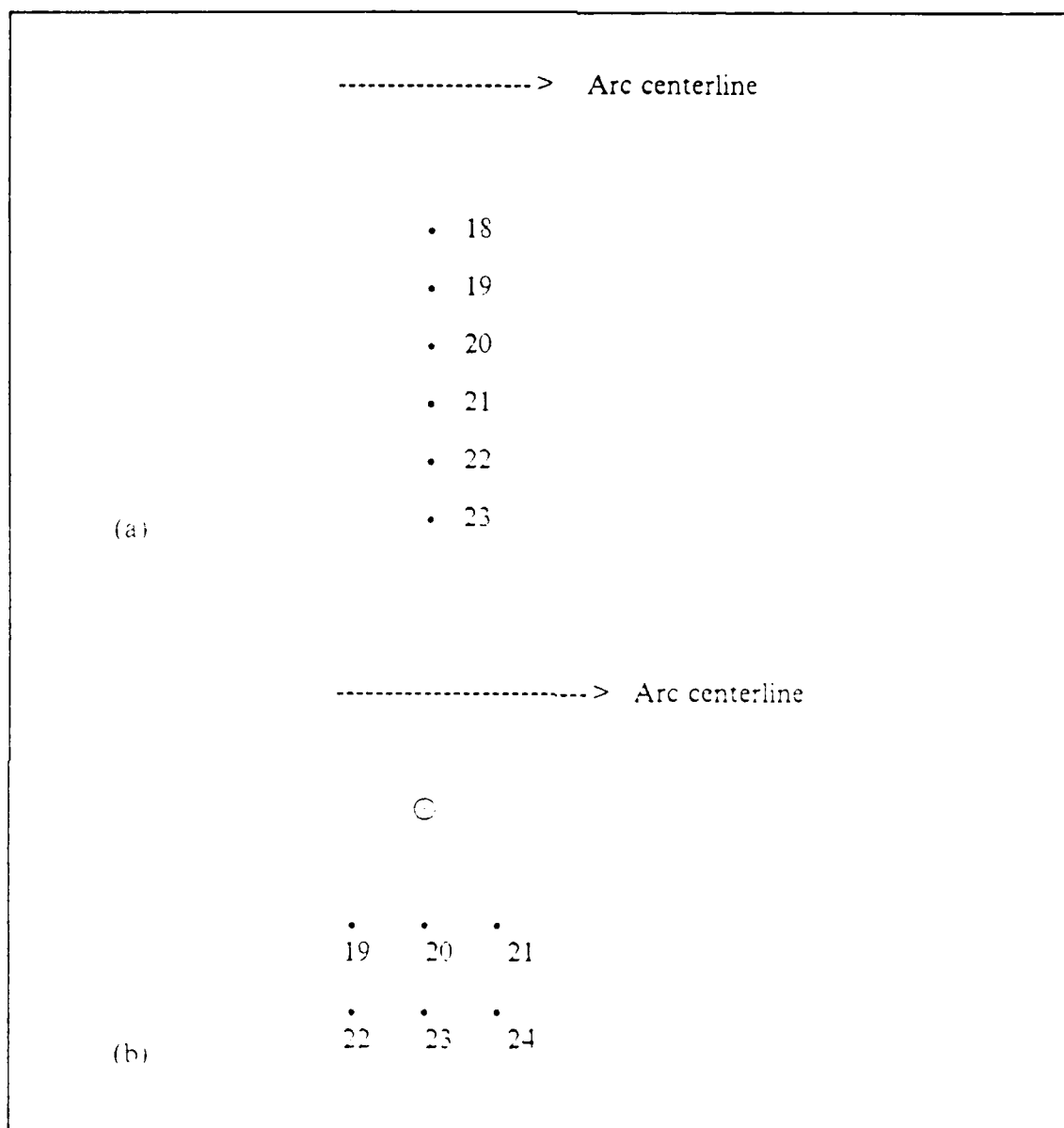


**Figure 7. Thermocouple locations:** (a) Baseline runs; offset 12mm, 3mm spacing  
(b) Surface flaw run; offset 10mm, 3mm spacing

The six thermocouple channels were scanned at 20 millisecond intervals for a period of about 40 seconds. The temperature versus time plots were observed on the terminal screen and also plotted for comparison with the computational model. A block diagram of the welding and data acquisition systems is provided in Figure 8.

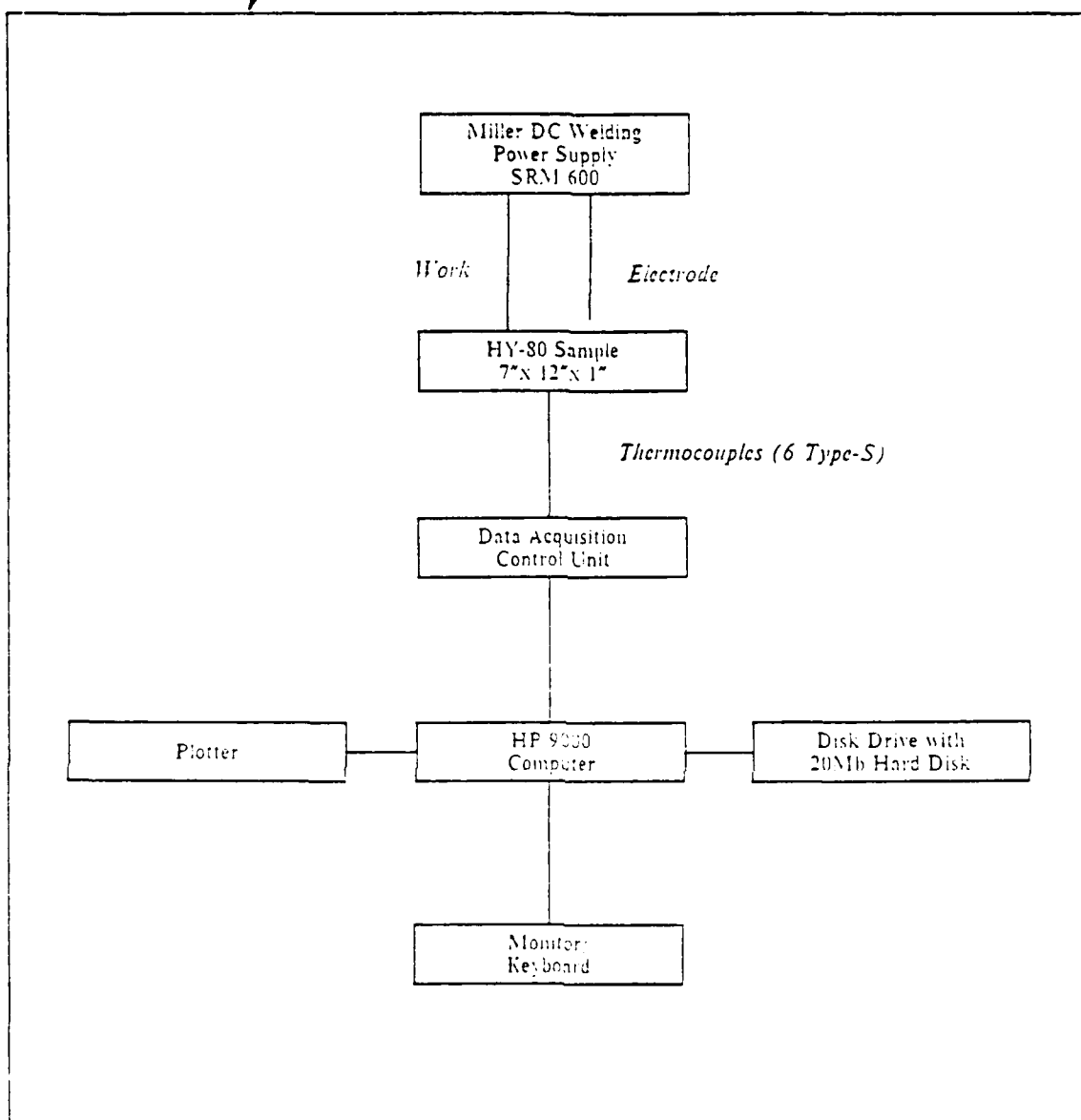


Figure 8. Welding and data acquisition systems

#### D. ARC EFFICIENCY DETERMINATION

The arc efficiency was measured by evaporating FC-72 when the just welded sample was placed in a tempering beaker of the fluid held near its saturation temperature. FC-72 is an inert dielectric liquid with a saturation temperature of about 56°C at one atmosphere pressure. It is often used in electronic cooling applications. The fluid was maintained at near saturation temperature by a heated recirculation bath with a flow

rate of about 1.5 gallons per minute of distilled water. The bath was a NESLAB Endocal model RTE-5B. The energy to change the phase of the mass of fluid lost plus the energy to raise the sample to the saturation temperature of the fluid was equated with the heat input to the metal. The energy used by the machine was calculated from voltage, current and time measurements during the sample weld. The amount of fluid lost due to steady evaporation during the course of the experiment was measured with a balance with a least count of one gram. The efficiency was then calculated by dividing the average power input by the machine indication of power. A block diagram of the system used for the efficiency measurement is shown in Figure 9.

#### **E. FUSION ZONE COMPARISON**

The size and shape of the fusion zone during the transient from arc initiation to quasi-steady state was determined by welding on the sample, cutting the bead at specified intervals, preparing the samples and photographing the prepared surfaces for measurements. The large plates were cut into sections small enough to fit into the sample cutter using a power hacksaw, then cut to the final size for analysis. The samples were prepared by sanding on 240, 320, 400 and 600 grit emery boards followed by polishing with 0.05 $\mu$  alumina and etching for about one minute with a 2% Nitrol solution. The fusion zones were photographed using Polaroid film through an optical microscope.

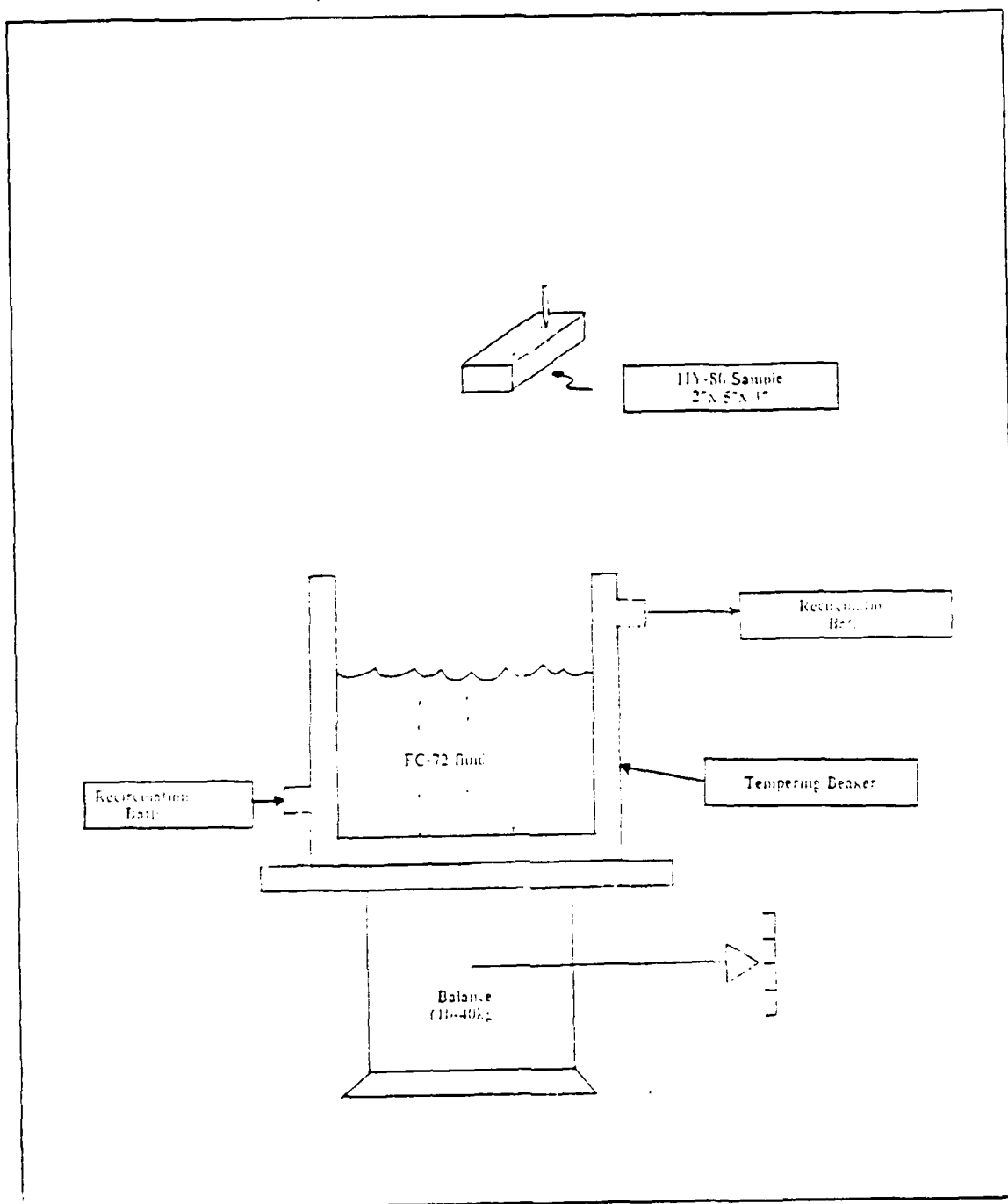


Figure 9. Efficiency determination system

## **IV. EXPERIMENTAL RESULTS**

### **A. DETERMINATION OF POWER INPUT TO SAMPLE**

The efficiency determination was made by two different methods. The first method was boiling FC-72 and measuring the mass of fluid lost by evaporation when the just welded sample was placed in the fluid. A second method was used because the results of the first were not consistent. The second method was matching the temperature-time plots obtained from the thermocouple output during baseline runs to the Rosenthal solution for the same thermophysical properties and arc velocities. Since the measurements used for the comparison were well away from the fusion zone, the Rosenthal model was an appropriate first approximation. The results are shown in Figure 10.

The inconsistent results of the phase change method may be explained in part by the relative magnitudes of the heat losses from the samples. The point furthest to the right in Figure 10 was obtained for about 14 seconds of welding, while the other two points were obtained from welds in excess of 35 seconds. For the latter two cases, the small sample size (2 inches by 5 inches by 1 inch thick) may have resulted in more conductive losses through the welding machine clamp as well as larger convective and radiative losses during welding and when the samples were moved to the tempering beaker.

The Rosenthal equation matching was more consistent. An explanation for the deviations from a linear response is the uncertainties in the experimental method which are discussed at the end of this chapter.

### **B. TEMPERATURE-TIME PLOT COMPARISONS**

Several welds at various power levels were made and temperature-time plots obtained from the thermocouple output. The Rosenthal solution was utilized to match the actual power input to the metal with the temperature-time plots. When the START2 program was run for the same parameters, the temperature-time plot did not match the experiment. In every case the model predicted much lower temperatures, though the shapes of the plots were similar. One source of the differences was that the Rosenthal solution does not include losses due to convection and radiation from the material as well as losses from the arc. Because the model applied the power directly to the sample and accounted for convective and radiative losses, a higher power than predicted by the Rosenthal solution would have been required to produce the same temperature-time



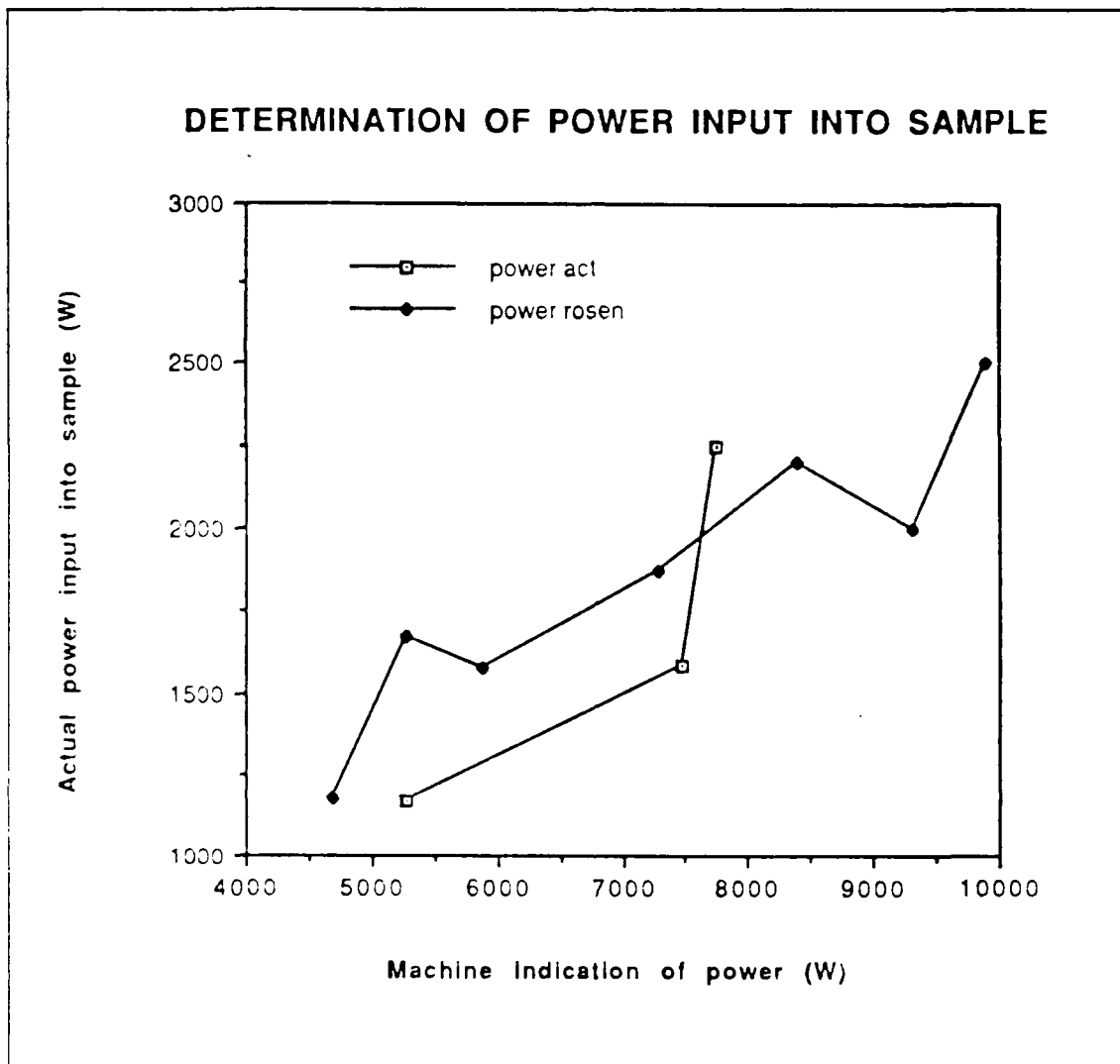


Figure 10. Welding process efficiency

plot. The results were therefore consistent with the assumptions of Rosenthal's analytic solution and the structure of the model.

### C. FUSION ZONE COMPARISON

The model under-predicted the size of the fusion zones during start-up as shown in Figures 12 through 15. Results of measurements of the actual fusion zone at positions corresponding to various times after initiation of the arc are represented in comparison to the model predictions in Table 1. Additionally, the tabular data were plotted and appear in Figure 15. It was noted that initially the modeled fusion zone was wider than the actual fusion zone. This result would imply that in the model the heat may have been input over too wide an area at the beginning of the weld. As the weld progressed the actual and modeled results followed the same trend on the plot. One difference observed was the model fusion zone reached quasi-steady state at about three seconds while the actual fusion zone reached a size and shape about which it oscillated after about five seconds.

**Table 1. FUSION ZONE COMPARISON:** Area ratio is the fusion zone area of the model divided by that of the sample.

Time (sec)	Sample Measurements		Model Predictions		Area Ratio
	width (mm)	depth (mm)	width (mm)	depth (mm)	
0.5	3.47	1.79	4.04	1.44	0.94
1.5	4.56	2.33	4.56	2.48	1.06
2.0	4.86	2.68	4.30	2.22	0.73
3.0	5.06	2.73	4.70	2.48	0.84
3.5	4.96	2.42	4.70	2.48	0.97
4.5	5.21	2.73	4.70	2.48	0.82
5.0	5.02	2.85	4.70	2.48	0.85
6.0	5.33	2.91	4.70	2.48	0.75
6.5	5.08	2.79	4.70	2.48	0.82
8.5	5.46	2.42	4.70	2.48	0.88

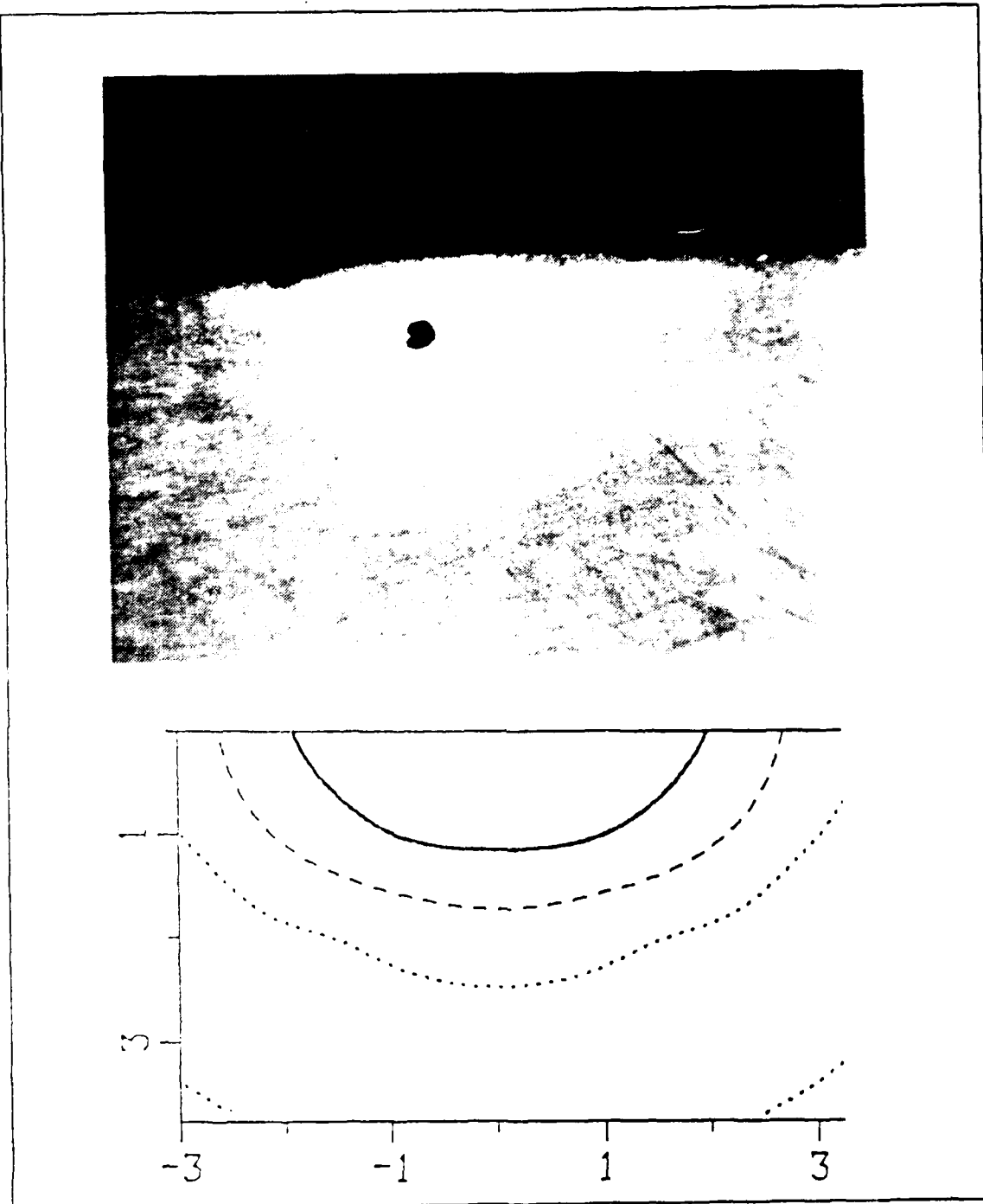


Figure 11. Fusion zone comparison at 0.5 seconds: (a) Photograph at 16X magnification (b) Model prediction at 16X magnification, scale in *mm*

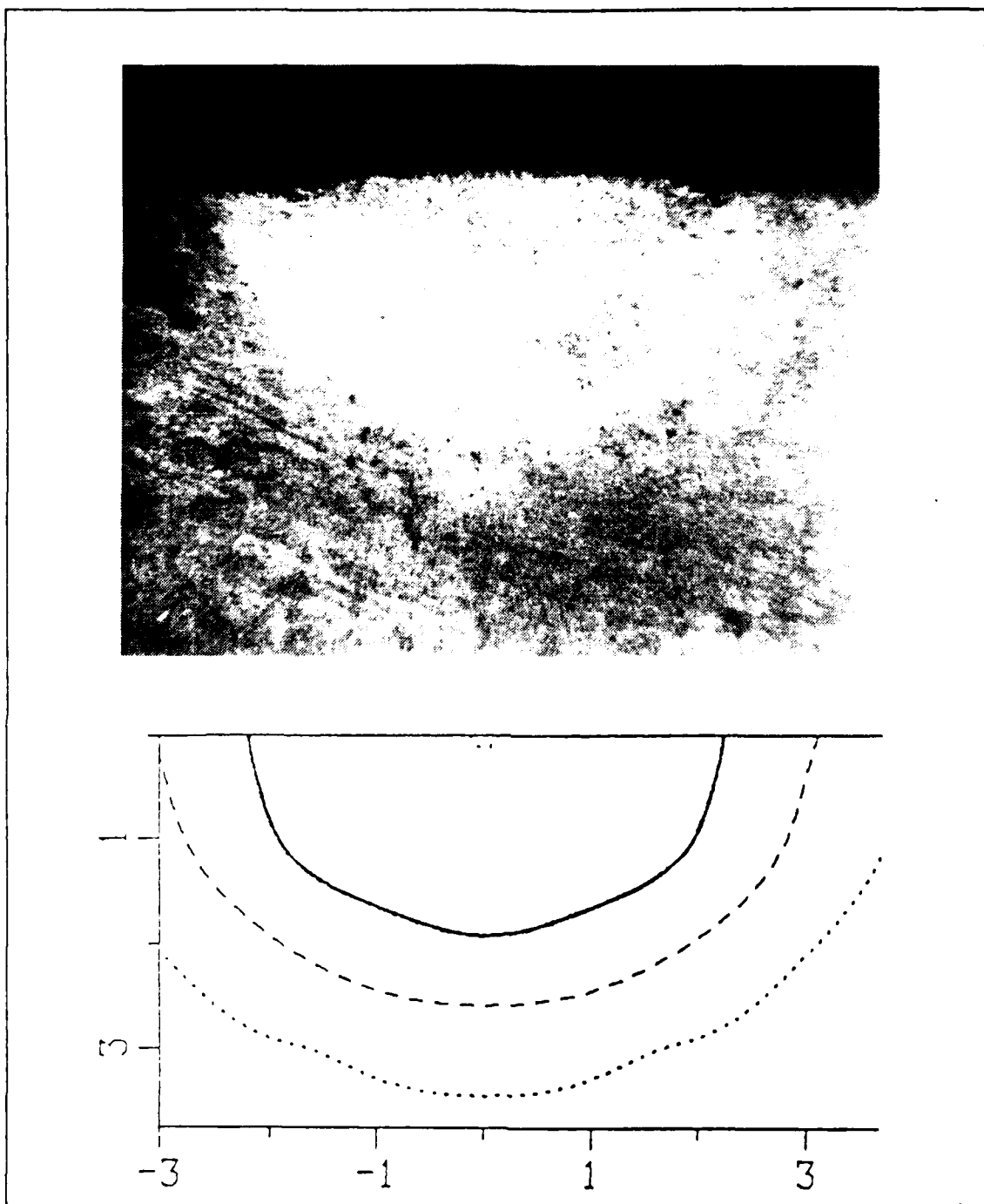


Figure 12. Fusion zone comparison at 1.5 seconds: (a) Photograph at 16X magnification (b) Model prediction at 16X magnification, scale in *mm*

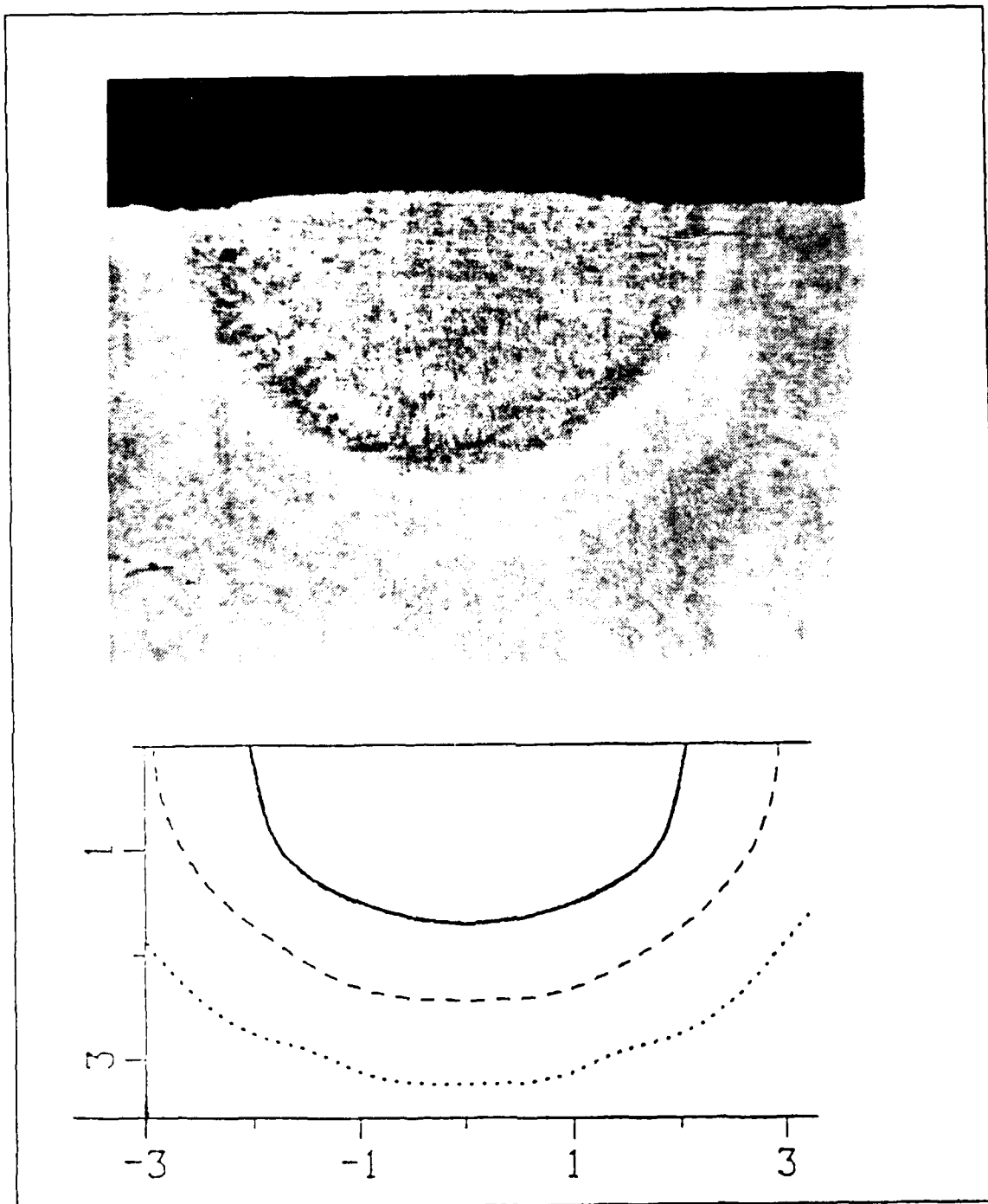


Figure 13. Fusion zone comparison at 2.0 seconds: (a) Photograph at 16X magnification (b) Model prediction at 16X magnification, scale in *mm*

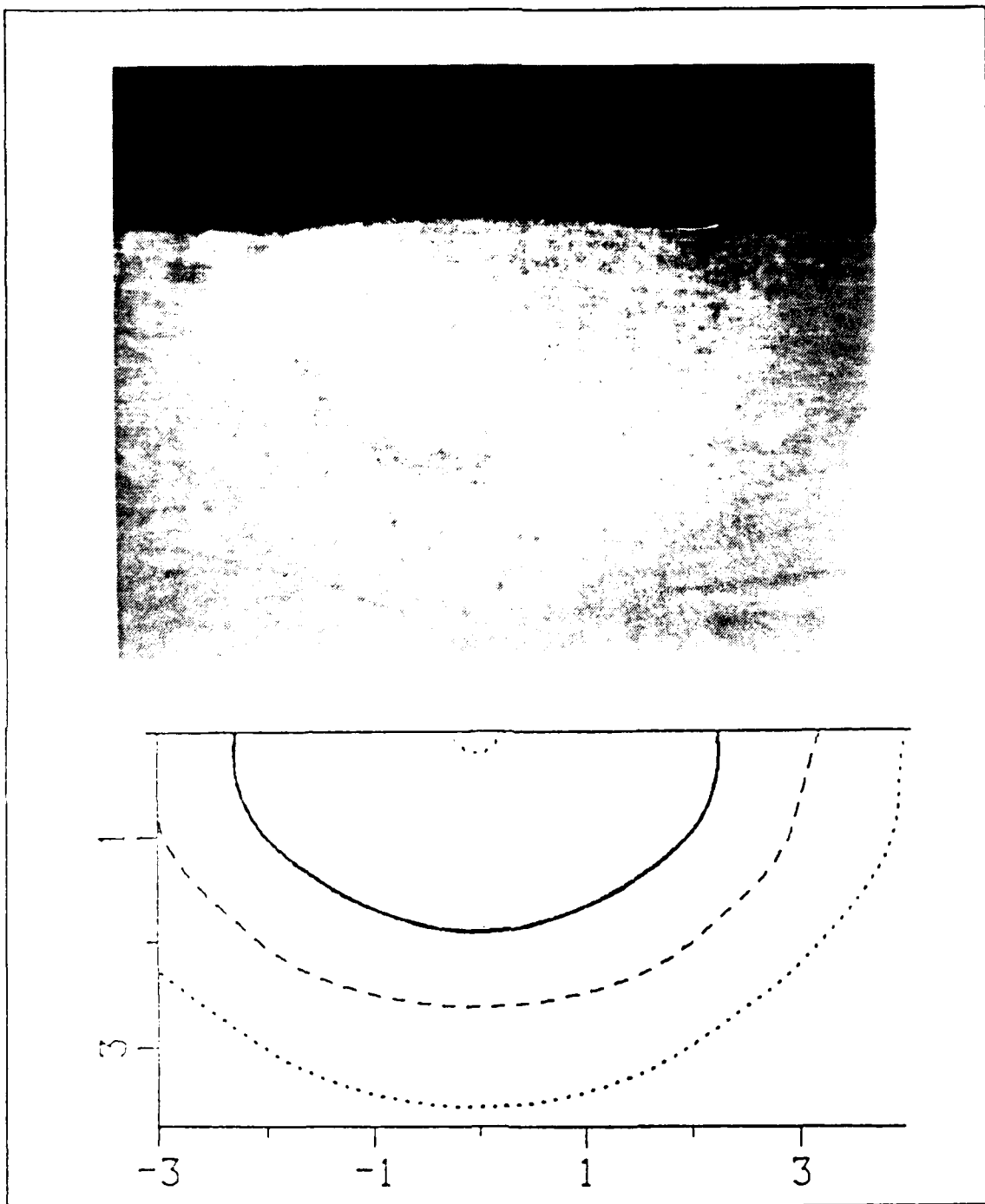


Figure 14. Fusion zone comparison at 3.0 seconds: (a) Photograph at 16X magnification (b) Model prediction at 16X magnification, scale in *mm*

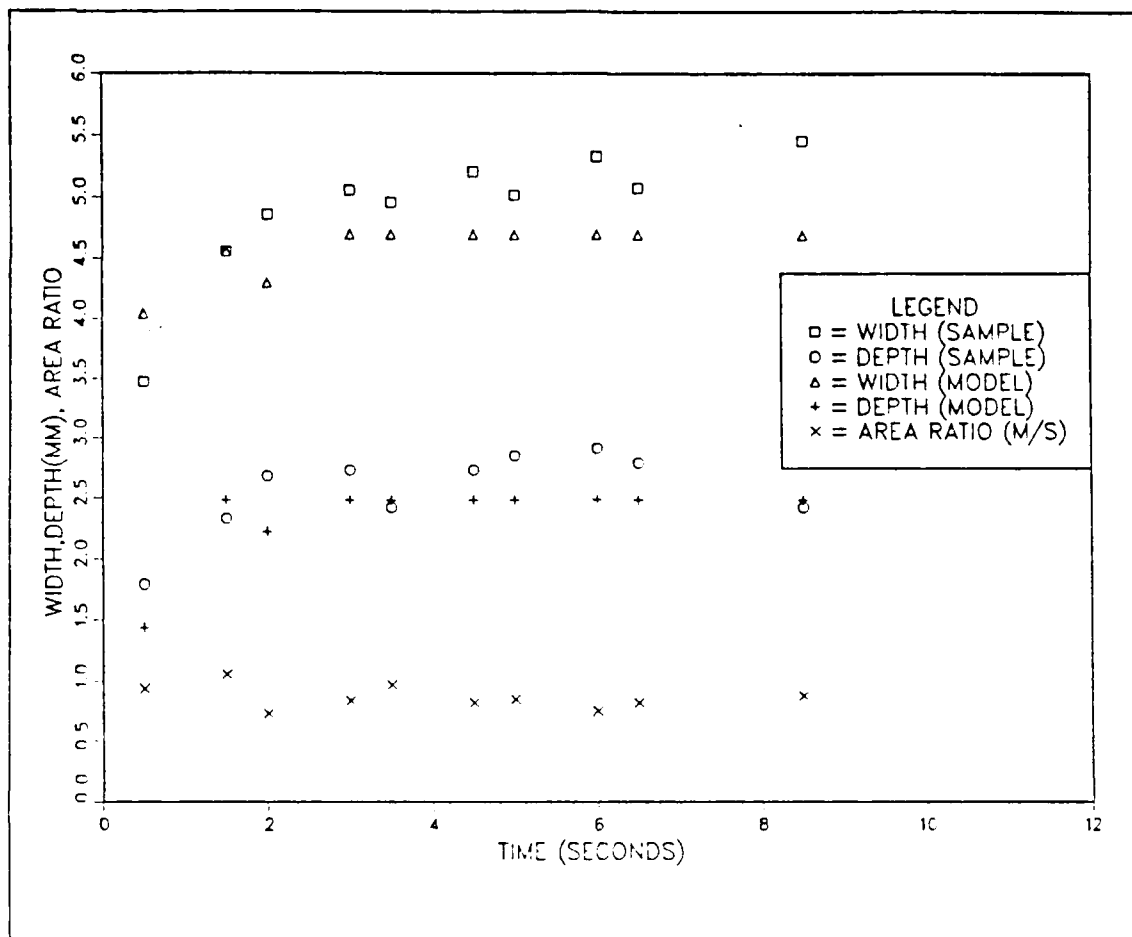


Figure 15. Fusion zone comparison over time

#### **D. SURFACE FLAW COMPARISON**

The temperature-time plots obtained from the thermocouple output for the surface flaw experiment were not as graphic in their representation of the flaw as the model. The thermocouple output for the surface flaw experiment is plotted in Figure 16. The model has the ability to show the temperature variations on the surface between the arc and the flaw. The limitations imposed by the use of surface mounted thermocouples precluded the same measurements in the experiment. The distortion of the thermal profile was evident, however, despite the noise in the thermocouple output. From this experiment it follows that a non-contact sensor capable of measuring the temperatures on the surface quite close to the arc, with a good sensitivity, would be more useful in validating the model capabilities in this area.

#### **E. EXPERIMENTAL UNCERTAINTIES**

Various components of the overall uncertainty are discussed in the following for the two phases of the experimental program.

##### **1. Efficiency determination**

The uncertainties in the procedure used to determine the power input to the sample during welding due to measurements only occurred in the following parameters: time, current, voltage, and mass of the fluid. The uncertainties for each parameter were:

time	0.5 seconds
current	10 amps
voltage	0.5 volts
mass	0.5 grams

The convective, radiative and conductive losses were unknown.

For the Rosenthal equation matching there was approximately a one millimeter uncertainty in the location of the thermocouples relative to the arc due to the error in marking the plate for thermocouple locations and to deviations of the arc from its intended path caused by slop in the gears in the traverse. An additional source of error was in the thermocouple output itself. There was approximately 5 to 10 K variation in the output as shown in Figure 17. The plot was representative of the thermocouple output on all channels with the welding machine off and the sample at ambient temperature for several days. The traverse speed was calibrated by timing the travel of the electrode over a distance of about 30 inches for each speed setting of the control. The



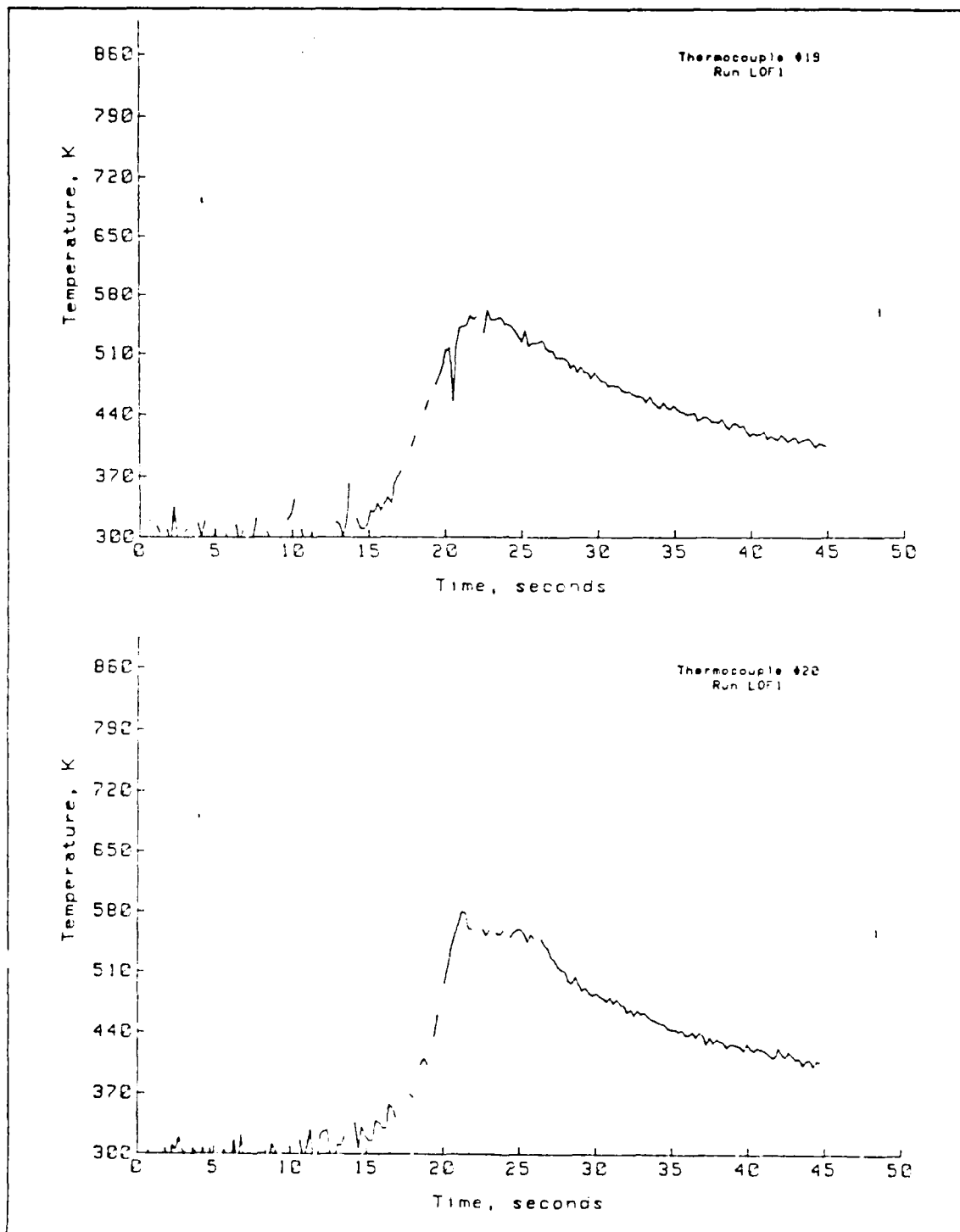


Figure 16. Surface flow temperature-time plots: Flaw of 4mm diameter and depth

response was linear but some error may have been encountered due to the coarse settings on the speed control.

## **2. Fusion zone comparison**

The fusion zone comparison samples were cut with a blade of about  $2mm$  width, which corresponded to about 0.5 seconds of elapsed time at a torch velocity of  $4.56 mm$  per second. Each sample was cut to about  $4.5mm$  thickness. The uncertainty in the measurements of the thickness was  $0.5 mm$ . The uncertainty in the measurements to determine the exact location of the arc at a given time was  $0.5mm$ . Combining these results, the actual time of the sample cut relative to the initiation of the arc had an uncertainty of about 0.25 seconds. The measurements of the fusion zone sizes on the photographs were highly accurate. The uncertainty of the measurements on the 16X magnified photographs was .03 inches. When correlated to the actual size of the sample, the uncertainty is less than  $0.05mm$ .

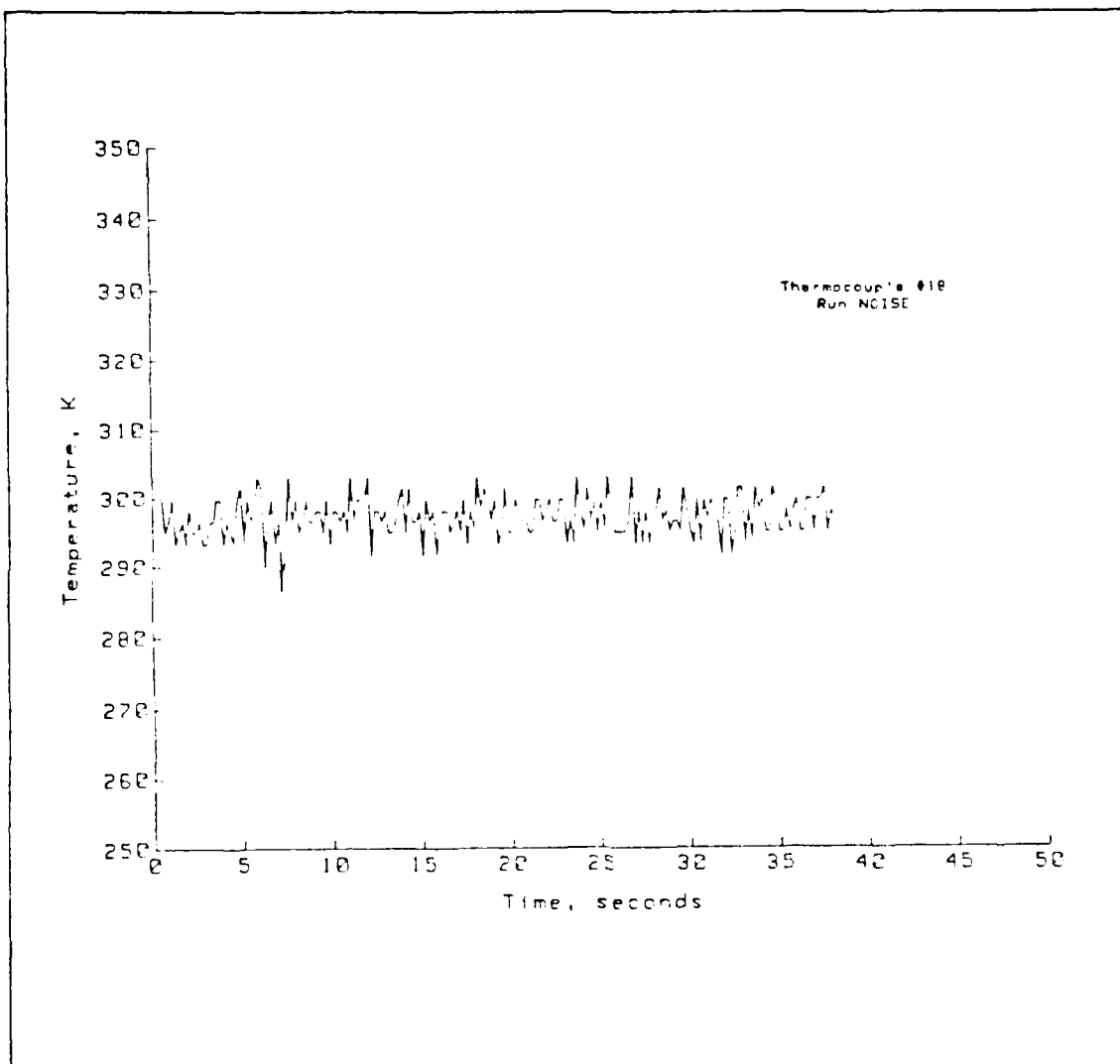


Figure 17. Noise in the thermocouple output

## **V. CONCLUSION AND RECOMMENDATIONS**

### **A. CONCLUSION**

The computational model written by Ule has been validated and shown to be useful in predicting the temperature distribution in a solid during autogenous welding. The ability to accurately predict the cooling rates during the weld cycle requires further development. The model has shown adaptability to different methods of heat input, which allow for study of different welding processes. The detectability of flaws in the material has been shown to be dependent on flaw location and composition. The need for an accurate non-contact surface temperature sensing system has been established.

### **B. RECOMMENDATIONS**

The current study has accomplished several objectives, yet further study and research will be required to determine the full capabilities and usefulness of the computational model.

#### **1. Cooling Rate Control**

Additional studies of the transient development of the weld pool during start-up and the solidification process during shutdown are required to determine the modifications necessary in the heat input distribution for the model to adequately predict the cooling rates at those points in the process. Through comparison of observed fusion zone sizes and shapes with model predictions, such a modification could be developed in an iterative process.

#### **2. Heat Input Distribution**

The double elliptical heat distribution should be studied and modified in order to obtain the proper major and minor axes of the ellipses and ratio of energy input in front of and behind the arc according to the process and material in question. The resulting information would allow the code to be used for the entire range of autogenous processes.

To minimize the complexity and subsequent run time of the code, convection in the weld pool should continue to be accounted for by use of a fictitiously high conductivity of the liquid phase and the arc digging should continue to be accounted for by the proper choice of heat input distribution.

### **3. Flaw Detectability**

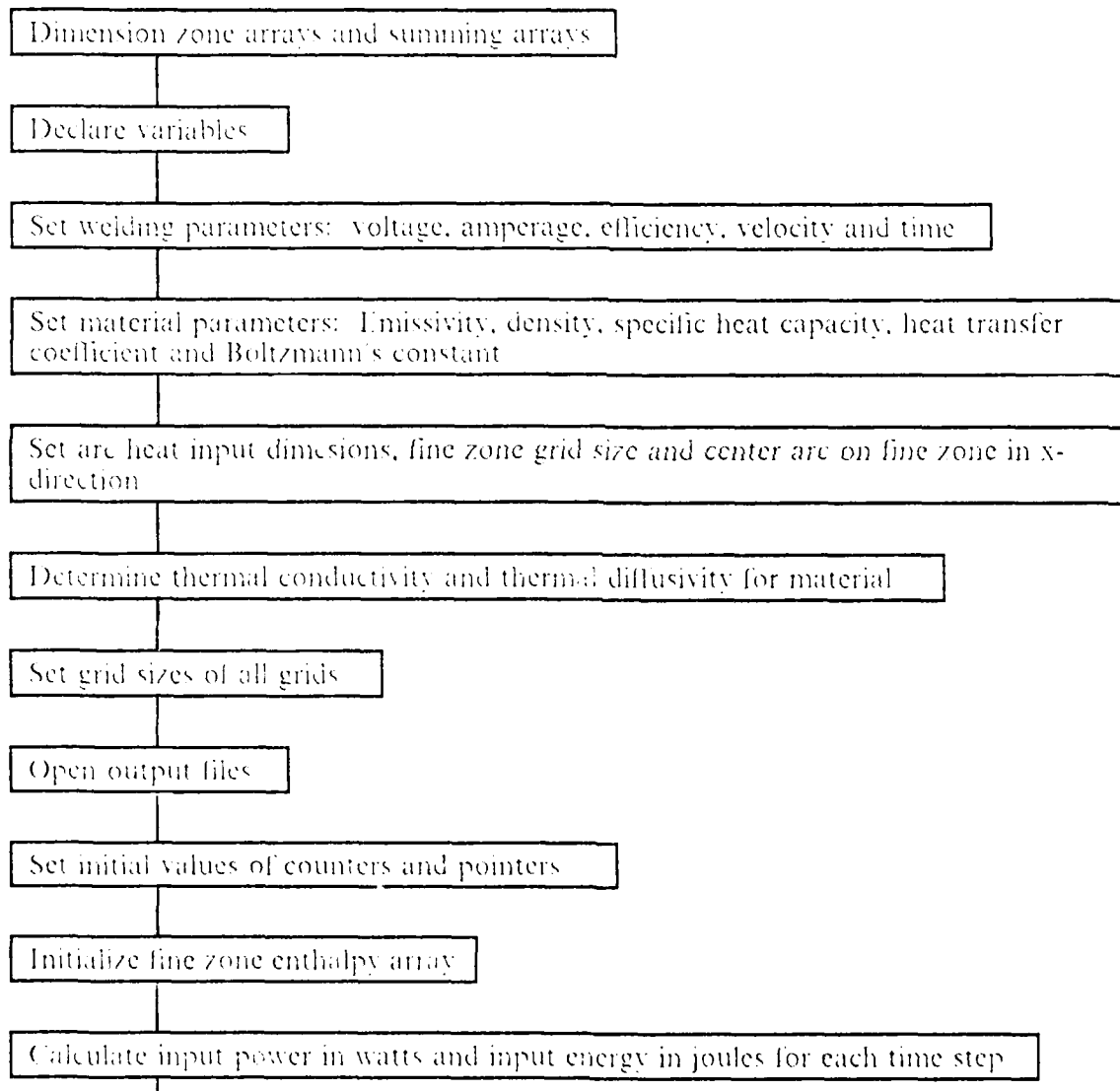
The detectability of flaws for various materials and process variables should be determined to assist in the preliminary design of a non-contact surface temperature sensing system by providing an estimate of the required sensitivity.

### **4. Temperature Sensing System**

The optimal non-contact surface temperature sensing system should be determined. A laser vision system has shown a capability of viewing the weld pool of a stationary arc. A qualitative determination of the shape and size of the fusion zone on the surface of the material for moving arcs should be made. This information could be applied to the model to assist in determining the heat input distribution shape, especially during start-up.

## APPENDIX A. FLOW CHART

A chart of the basic program flow was constructed to aid in the understanding of the code structure and execution.



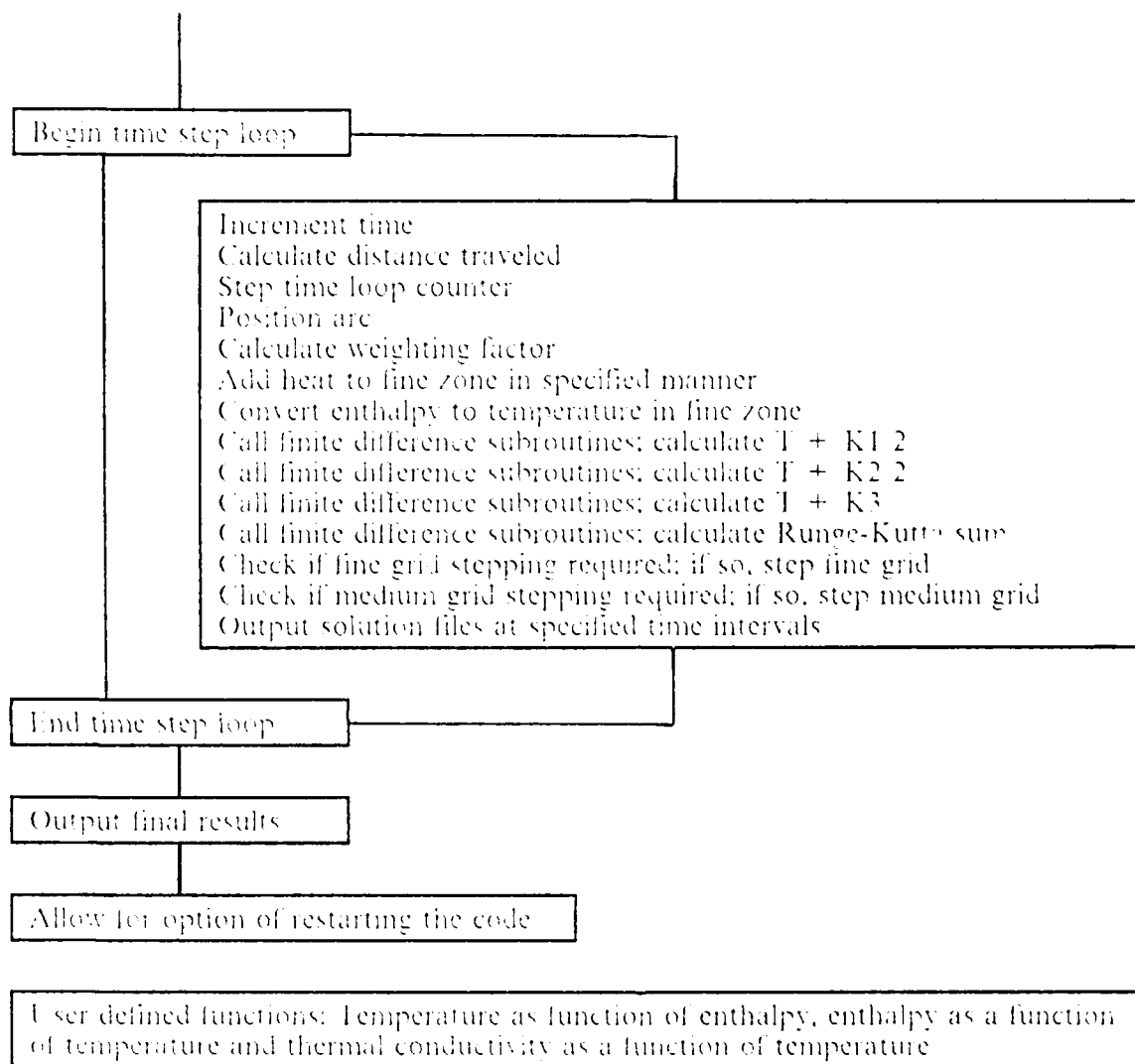


Figure 18. Program Flow Chart

## APPENDIX B. MODIFIED PROGRAMS

The portions of codes that were changed are provided along with the corresponding portions of Ule's codes for comparison. A list of the additional variables used in each new section of code is also provided.

### A. BASIC MODIFICATIONS

#### 1. START2 Program Modified Sections

```
SIGMA = 5.67E-8
EPSIL = 0.82
RHO = 7890
CPSP = 536
HF = 25.0
HM = 10.0
HC = 10.0

C
A1 = 4.0
B1 = 4.0
C1 = 4.0
SPACE = 1.0
XARC = 14.0

C
KAPPA = FK(300.0)
ALPHA = KAPPA/(RHO*CPSP)

C
DELXF = SPACE
DELXM = 3.0 * SPACE
DELXC = 3.0 * DELXM
DELYF = SPACE
DELYM = 3.0 * SPACE
DELYC = 3.0 * DELYM
DELZF = SPACE
DELZM = 3.0 * SPACE
DELZC = 3.0 * DELZM

C BOUNDARY CONDITION COEFFICIENTS

FO(1)=ALPHA*DELTA/((DELXC*DELYC*1.0E-3**2)
BI(1)=(2.0/3.0)*HC*DELXC*1.0E-3/KAPPA

FO(2)=ALPHA*DELTA/((DELXM*DELYM*1.0E-3**2)
BI(2)=2.0*HM*DELXM/KAPPA

FO(3)=DELTA/(DELXF*1.0E-3)**2
BI(3)=EPSIL*SIGMA*2.0*DELTA/DELZF
BI(4)=HF*2.0*DELTA/DELZF

C CALCULATE THE RUNGE-KUTTA APPROXIMATION
```



```

DO 10 M=1,NDIV
  TIME=FLOAT(NINT(100.*(TIME+DELT)))/100.
  DIS=TIME*VEL
  N=N+1

```

C POSITION HEAT SOURCE, CALCULATE VOLUME WEIGHTING FACTOR 'ENERGY'

```

  YARC=DIS+73-NB*9-NC*3
  ENERGY = 0.0
  I1 = INT (A1/SPACE)
  XLIML = XARC - I1-1
  XLIMU = XARC + I1+1
  J1 = INT(B1/SPACE)
  YLIML = INT(YARC) - J1 - 2
  YLIMU = INT (YARC) + J1 + 2
  K1 = INT(C1/SPACE) + 1
  DO 300 I = XLIML,XLIMU
    XE = ((I-XARC)/A1)**2
    DO 200 J = YLIML,YLIMU
      YE = ((J-YARC)/B1)**2
      DO 100 K = 1,K1
        ZE = ((K-1)/C1)**2
        EXPON = XE+YE+ZE
        IF(EXPON.GT.1.0) GO TO 200
        IF(K.EQ.1) THEN
          VOL = 0.5 * (SPACE*1.0E-3)**3
        ELSE
          VOL = (SPACE*1.0E-3)**3
        ENDIF
        ENERGY = ENERGY + VOL * EXP(-3.0 * EXPON)
      100 CONTINUE
    200 CONTINUE
  300 CONTINUE

```

C ADD THE HEAT FROM THE ARC HERE USING A SIMILAR DO LOOP  
 C CONSTRUCTION AS ABOVE!

```

  DO 600 I = XLIML,XLIMU
    XE = ((I-XARC)/A1)**2
    DO 500 J = YLIML,YLIMU
      YE = ((J-YARC)/B1)**2
      DO 400 K = 1,K1
        ZE = ((K-1)/C1)**2
        EXPON = XE+YE+ZE
        IF(EXPON.GT.1.0) GO TO 500
        C(I,J,K)=C(I,J,K)+EXP(-3.0*EXPON)*Q/ENERGY
      400 CONTINUE
    500 CONTINUE
  600 CONTINUE

```

## 2. Variable List

The following variables were added to all programs to allow easier input of different heat input schemes and to allow for the study of different materials. The grid size parameters were also coded for future use if it was desired to change grid size. All variables are given in standard SI units unless otherwise noted.

<b>SIGMA</b>	Boltzmann's constant
<b>EPSIL</b>	Emmissivity of the surface
<b>RHO</b>	Density of the material
<b>CPSP</b>	Specific heat capacity
<b>HF</b>	Heat transfer coefficient for the fine zone surfaces
<b>HM</b>	Heat transfer coefficient for the medium zone surfaces
<b>HC</b>	Heat transfer coefficient for the coarse zone surfaces
<b>A1</b>	Radius of heat input in x-direction in millimeters
<b>B1</b>	Radius of heat input in positive y-direction in millimeters
<b>B2</b>	Radius of heat input in negative y-direction in millimeters
<b>C1</b>	Radius of heat input in z-direction in millimeters
<b>SPACE</b>	Node spacing in the fine zone in millimeters
<b>XARC</b>	Position of the arc in the fine zone in x-direction
<b>KAPPA</b>	Thermal conductivity
<b>ALPHA</b>	Thermal diffusivity
<b>DELXF</b>	Control volume length in x-direction in fine zone
<b>DELXM</b>	Control volume length in x-direction in medium zone
<b>DELXC</b>	Control volume length in x-direction in coarse zone
<b>DELYF</b>	Control volume length in y-direction in fine zone
<b>DELYM</b>	Control volume length in y-direction in medium zone
<b>DELYC</b>	Control volume length in y-direction in coarse zone
<b>DELZF</b>	Control volume length in z-direction in fine zone
<b>DELZM</b>	Control volume length in z-direction in medium zone
<b>DELZC</b>	Control volume length in z-direction in coarse zone
<b>FO(1)</b>	Fourier number in the coarse zone
<b>BI(1)</b>	Biot number in the coarse zone
<b>FO(2)</b>	Fourier number in the medium zone
<b>BI(2)</b>	Biot number in the medium zone

FO(3)	Fourier number in the fine zone
BI(3)	Biot number in the fine zone (for radiation)
BI(4)	Biot number in the fine zone (for convection)
ENERGY	Summing variable for the total energy input in a time step
II	Converts radius of arc input to nodal value for x-direction
XLIML	Lower limit of x-direction input of heat
XLIMU	Upper limit of x-direction input of heat
J1	Converts radius of arc input to nodal value for y-direction
YLIML	Lower limit of y-direction input of heat
YLIMU	Upper limit of y-direction input of heat
K1	Converts radius of arc input to nodal value for z-direction
XE	Contribution to exponent in Gaussian distribution from x-direction
YE	Contribution to exponent in Gaussian distribution from y-direction
ZE	Contribution to exponent in Gaussian distribution from z-direction
EXPON	Value of exponent in the Gaussian distribution expression
VOL	Volume of the node being evaluated in cubic meters

### 3. Original WELD Program Sections

The following are sections of program from the original version written and used by Ule [Ref. 12: pp. 85-86].

```

DATA XZ/. 1433987,. 2870068,
*. 4352117,. 5,. 4352117,. 2870068,. 1433987,. 2184978,. 4373148,
*. 6631358,. 76118543,. 6631358,. 4373148,. 2184978,. 096619,. 1933793,
*. 2932366,. 3368896,. 2932366,. 1933793,. 096619/
DATA A,B/8046*300.0/,C/5832*1. 14237E8/,ASUM,BSUM/8046*0.0/
*,AOUT,BOUT/8046*0.0/,CSUM/5832*0. /,COUT/5832*0. /

C INITIAL DATA BLOCK FOR STARTING A PROBLEM, SET PROBLEM LENGTH AND
C ARC PARAMETERS

FINI = 10.0
VOLT=30.
AMP=265.
EFF=. 32
VEL=4.

C OPEN THE OUTPUT FILES

OPEN(1,FILE='SURF',STATUS='NEW',FORM='UNFORMATTED')
OPEN(2,FILE='FINAL',STATUS='NEW',FORM='UNFORMATTED')
```

```

OPEN(3,FILE='CUT',STATUS='NEW',FORM='UNFORMATTED')
OPEN(4,FILE='HIST',STATUS='NEW',FORM='UNFORMATTED')

```

C THE INITIAL CONDITIONS: NUMBER OF DIVISIONS, TIME STEP, TIME  
 C AND ARC LOCATION, ETC.

```

NDIV=FINI*100
DELT=.01
TIME=0.
STEP=3.
OUT=.49
N=0
BSTEP=0
CSTEP=0
NB=3
NC=10
QDENSE=7.134346E-9
TINF=300.0

```

C WELD PARAMETERS

```

QDOT=EFF*VOLT*AMP
Q=QDOT*DELT

```

C BOUNDARY CONDITION COEFFICIENTS

```

FO(1)=DELT*.1636
FO(2)=DELT*1.4722
FO(3)=DELT*1000000.
BI(1)=.001132
BI(2)=.001132
BI(3)=DELT*.00009299
BI(4)=DELT*50000.

```

C CALCULATE THE RUNGE-KUTTA APPROXIMATION

```

DO 10 M=1,NDIV
  TIME=TIME+DELT
  DIS=TIME*VEL
  N=N+1

```

C POSITION HEAT SOURCE AND CALCULATE VOLUME WEIGHTING FACTOR SUM'

```

  YARC=VEL*TIME+73-NB*9-NC*3
  SUM=0.
  DO 1 J=7,23
C    IF ((J-YARC).GT.(0.0)) THEN **** LINES ALLOWED SHAPING THE ARC
      SUM=SUM+QDENSE/4.*EXP(-.10625*((J-YARC)**2))
C    ELSE
C      SUM=SUM+QDENSE/10.*EXP(-.017*((J-YARC)**2))
C    ENDIF
  1 CONTINUE
  SUM=SUM/Q

```

C ADD THE HEAT FROM THE ARC

```

DO 2 J=7,23
C   IF ((J-YARC).GT.(0.0)) THEN  ***** LINES ALLOWED SHAPING THE ARC
      Y=.25*EXP(-.10625*((J-YARC)**2))
C   ELSE
C      Y=.1*EXP(-.017*((J-YARC)**2))
C   ENDIF
      DO 2 I=11,17
        DO 2 K=1,3
          C(I,J,K)=C(I,J,K)+Y*XZ(I-10,K)/SUM
2 CONTINUE

```

## LIST OF REFERENCES

1. Rosenthal, D., "The Theory of Moving Sources of Heat and its Application to Metal Treatments", *Transactions ASME*, v. 68, November 1946.
2. Moody, W.V., *Automatic Welding Control Using a State Variable Model*, Master's Thesis, Massachusetts Institute of Technology, Cambridge, MA, 1979.
3. Eagar, T.W. and Tsai, N.S., "Temperature Fields Produced by Traveling Distributed Heat Sources," *Welding Journal*, v.62, December 1983.
4. Goldak, J., Chakravarti, A., and Bibby, M., "A New Finite Element Model for Welding Heat Sources," *Metallurgical Transactions B*, v.15B, June 1984.
5. Kou, S. and Sun, D.K., "Fluid Flow and Weld Penetration in Stationary Arc Welds," *Metallurgical Transactions A*, v.16A, February 1985.
6. Tsai, N.S. and Eagar, T.W., "Distribution of the Heat and Current Fluxes in Gas Tungsten Arcs," *Metallurgical Transactions B*, v.16B, December 1985.
7. Kou, S. and Wang, Y.H., "Computer Simulation of Convection in Moving Arc Weld Pools," *Metallurgical Transactions A*, v.17A, December 1986.
8. Sandia National Laboratories Report, *GTA Weld Penetration and the Effects of Deviations in Machine Variables*, by W.H. Giedt, July 1987.
9. Oreper, G.M. and Szekely, J., "A Comprehensive Representation of Transient Weld Pool Development in Spot Welding Operations," *Metallurgical Transactions A*, v.18A, July 1987.
10. Lu, M.J. and Kou, S., "Power and Current Distributions in Gas Tungsten Arcs," *Welding Journal*, February 1988.

11. Zacharia, T., Eraslan, A.H., and Aidun, D.K., "Modeling of Autogenous Welding," *Welding Journal*, March 1988.
12. Ule, R.L., "A Study of the Thermal Profiles During Autogenous Arc Welding," M.S. and M.E. Thesis, Naval Postgraduate School, Monterey, CA, March 1989.
13. Incropera, F.P. and DeWitt, D.P., *Introduction to Heat Transfer*, John Wiley & Sons, Inc., 1985.

## BIBLIOGRAPHY

Baker, H.D., Ryder, E.A. and Baker, N.H., *Temperature Measurement in Engineering*, Omega Press, 1975.

Benzinger, T.H. and Kitzinger, C., "Direct Calorimetry by Means of the Gradient Principle," *The Review of Scientific Instruments*, v.12, December 1949.

Idaho National Engineering Laboratory Report, *Electronic Imaging Technique for Welding and Other High-Luminosity Processes*, by J.O. Bolstad, September 1987.

Jhaveri, P., Moffatt, W.G. and Adams, C.M., "The Effect of Plate Thickness and Radiation of Heat Flow in Welding and Cutting," *Welding Journal*, January 1962.

Kou, S. and Wang, Y.H., "Three-Dimensional Convection in Laser Melted Pools" *Metallurgical Transactions A*, v.17A, December 1986.

Kraus, H.G., "Experimental Measurement of Stationary SS304, SS316L and 8630 GTA Weld Pool Surface Temperatures," *Welding Journal*, 1989.

Lancaster, J.F., *Metallurgy of Welding*, Allen & Unwin Ltd, 1987.

Lu, M.J. and Kou, S., "Power Inputs in Gas Metal Arc Welding of Aluminum--Part 2," *Welding Journal*, November 1989.

McKelliget, J. and Szekely, J., "Heat Transfer and Fluid Flow in the Welding Arc," *Metallurgical Transactions A*, v.17A, July 1986.

McLay, R. and Carey, G.F., "Coupled Heat Transfer and Viscous Flow, and Magnetic Effects in Weld Pool Analysis," *International Journal for Numerical Methods in Fluids*, v.9, 1989.



Nagarajan, S., Chen, W.H. and Chin, B.A., "Infrared Sensing for Adaptive Arc Welding," *Welding Journal*, November 1989.

Niles, R.W. and Jackson, C.E., "Weld Thermal Efficiency of the GTAW Process," *Welding Journal*, v.54, January 1975.

Zacharia, T., David, S.A., Vitek, J.M., and Debroy, T., "Heat Transfer during Nd:Yag Pulsed Laser Welding and Its Effect on Solidification Structure of Austenitic Stainless Steels," *Metallurgical Transactions A*, v.20A, May 1989.

Zacharia, T., Eraslan, A.H., and Aidun, D.K., "Modeling of Non-Autogenous Welding," *Welding Journal*, January 1988.

## INITIAL DISTRIBUTION LIST

		No. Copies
1.	Defense Technical Information Center Cameron Station Alexandria, VA 22304-6145	2
2.	Library, Code 0142 Naval Postgraduate School Monterey, CA 93943-5002	2
3.	E.A. Metzbower Naval Research Laboratory Washington, D.C. 20375-5000	1
4.	Department Chairman, Code 69 Department of Mechanical Engineering Naval Postgraduate School Monterey, CA 93943-5000	1
5.	Yogendra Joshi, Code 69Ji Naval Postgraduate School Monterey, CA 93943-5000	2
6.	Richard Morris Code 2815 David Taylor Research Laboratory Annapolis, MD 21402	1
7.	RADM Roger Horne SEA - 05 Naval Sea Systems Command Washington, D.C. 20362-5101	1
8.	RADM Thomas W. Evans SEA - 92R Naval Sea Systems Command Washington, D.C. 20362-5101	1
9.	Naval Engineering Curricular Office Code 34 Naval Postgraduate School Monterey, CA 93943-5000	1
10.	Eugene B. Sedy 16409 N.E. 122 St. Redmond, WA 98052	2